TIME DOMAIN ELECTROMAGNETIC MIGRATION

by

Oleg Nikolaevich Portniaguine

A thesis submitted to the faculty of
The University of Utah
in partial fulfillment of the requirements for the degree of

Master of Science

in

Geophysics

Department of Geology and Geophysics

The University of Utah

August 1995

THE UNIVERSITY OF UTAH GRADUATE SCHOOL

SUPERVISORY COMMITTEE APPROVAL

of a thesis submitted by

Oleg Portniaguine

This thesis has been read by each member of the following supervisory committee and by majority vote has been found to be satisfactory.

Chair: Michael S. Zhdanov

Gerard T. Schuster

Alan C. Tripp

THE UNIVERSITY OF UTAH GRADUATE SCHOOL

FINAL READING APPROVAL

To the Graduate Council of the University of Utah:

I have read the thesis of [redacted] Nikolaevich [redacted] in its final form and have found that (1) its format, citations, and bibliographic style are consistent and acceptable; (2) its illustrative materials including figures, tables, and charts are in place; and (3) the final manuscript is satisfactory to the supervisory committee and is ready for submission to The Graduate School.

[redacted]
Date

[redacted]
Michael S. Zhdanov
Chair: Supervisory Committee

Approved for the Major Department

[redacted]

Approved for the Graduate Council

[redacted]
Ann W. Hart
Dean of The Graduate School

ABSTRACT

This thesis develops a new approach to processing transient electromagnetic data. This approach is called *time domain electromagnetic migration (TDEMM)*. The migration method is specifically designed to process multidimensional time-domain electromagnetic data in order to obtain a resistivity image of subsurface structure which clearly indicates the spatial location of the targets and estimates their anomalous conductivity.

The theoretical foundations of migration, a model study illustrating the method's stability and resolution, and an application of the migration procedure to real data interpretation are subsequently considered in this work.

CONTENTS

LIST OF FIGURES

ACKNOWLEDGEMENTS

I thank the Consortium on Electromagnetic Modeling and Inversion at the Department of Geology and Geophysics, University of Utah, for providing support for this work.

I also thank my adviser, Dr. M.S. Zhdanov, for sharing the ideas and directing this research.

Special thanks to my colleagues, Dr. P. Traynin for his help with handling and visualizing the data, and E. Tartaras for his contribution to model calculations.

I am grateful to Dr. H. D. MacLean for providing the TDEM data and fruitful discussions of the results of migration and resistivity imaging, and Dr. A.C.Tripp for discussions, comments, and corrections.

I appreciate Dr. G.T. Schuster for the ideas and suggestions about future development of this work.

1. INTRODUCTION

1.1 Time domain electromagnetic soundings

Transient electromagnetic methods are widely used in exploration geophysics and environmental studies. These are inexpensive and reliable nondestructive methods of subsurface and borehole investigations. Transient electromagnetic soundings can indicate the location of structures with anomalous conductivities with respect to the surrounding medium.

Classification of transient sounding methods is based on transmitter type and survey design. The transmitter is usually a square or circular loop or coil, excited by an abruptly terminated current. Surface and borehole surveys can be done in many different ways. In the *fixed transmitter technique* the induced magnetic field is measured at many receiving points, located at a variable distance from the transmitter. A second survey possibility, the *slingram mode*, requires the receiver and transmitter to be a fixed distance apart, moving together along the profile.

Transient electromagnetic data are most often interpreted using conventional one-dimensional (1D) inversion techniques, or approximate, fast imaging techniques.

The theory of 1D inversion is based on fitting the theoretical response from a 1D structure to the real data in a least-square sense (Farquharson and Oldenburg, 1993). It is conventionally applied to every survey point. Combining 1D images together forms the resistivity-cross section.

Fast resistivity imaging techniques have been developed in (Eaton and Hohmann, 1989; Macnae and Lamontagne, 1987; Barnett, 1981). The majority of these papers have been based on equating the transient response, measured at the surface of the earth, to the electromagnetic (EM) field of current filament images of the source. This approach was originated in the pioneering work of Nabighian (1979), which describes the transient currents diffusing into the earth as a system of "smoke rings" blown by

the transmitting loop into the earth.

1.2 Introducing time domain electromagnetic migration

This thesis focuses on an approach to processing transient EM data, based on downward data extrapolation in reverse time. This method is called *time domain electromagnetic migration.* The principles of EM migration have been formulated originally in the pioneering works of Zhdanov and Frenkel (1983) and they have been developed in several publications by Zhdanov and coauthors (Zhdanov and Frenkel, 1983a,b; Zhdanov and Podchufarov, 1988; Zhdanov et al., 1988; Zhdanov and Keller, 1994).

The migration method is a multidimensional imaging method, which is the major advantage in comparison with the conventional 1D inversion and the "smoke ring" approaches. In this thesis a 2D migration algorithm is considered, but it can be readily generalized to the 3D case.

Comparison of migration with 1D imaging is done by Traynin (1995). This work concludes that the migration method has better resolution of localized bodies. However, the "smoke ring" imaging could be used for an estimation of background resistivity.

In this work we modified a preceding time domain electromagnetic migration algorithm, and developed an effective numerical method and a computer code for resistivity imaging. We then tested the migration method on a set of numerical models and real TDEM data.

Electromagnetic migration is similar in many aspects to seismic migration (Zhdanov et al., 1988; Claerbout, 1985) but differs in that electromagnetic migration is done on the basis of a diffusion equation rather than a wave equation. Seismic migration is based on downward continuation of the source field and the scattered field on the basis of a wave equation. At zero time the phases of the incident and the scattered fields are typically coincident at the boundary of the scatterer, and the ratio of incident and scattered field amplitudes is proportional to the reflection

coefficient for this boundary. The wave field backward continuation problem could be formulated as a boundary value problem for the same wave equation, but with a changed boundary condition for the vertical derivative of the seismic field. Reversing the time affects only the boundary condition, but not the form of the wave equation. Thus, upward and downward continuation of the wave field do not differ much from one another. Physically, propagation of seismic waves in rocks is characterized by some attenuation, with a large amplitude decrease caused by geometrical spreading and losses from reflections. In fact, the wave equation which is successfully used in most cases, does not contain an attenuative factor at all. That is why it is relatively easy to backward propagate the seismic field.

It was demonstrated in the literature that seismic migration can be treated as the first iteration in the process of minimizing the waveform misfit functional (Tarantola, 1987). This also can be shown for the electromagnetic high-frequency field (Cai et al., 1995). We expect that the same type of generalization can be developed for the quasi-stationary EM field as well. However, this consideration lies outside the framework of this thesis.

Electromagnetic field propagation is characterized by strong attenuation. For low frequencies the attenuation dominates over the wave propagation, which provides the basis for a quasi-stationary approximation that describes low-frequency electromagnetic field propagation as a pure diffusion process. Although the same downward continuation could be done on the basis of the diffusion equation for the electromagnetic field, such a transformation would be unstable, for it dramatically amplifies high frequencies. To avoid instability, *electromagnetic migration* is defined as downward continuation of the diffusive field in reverse time. This transformation correctly reconstructs only the phase of the backward propagating field, but not the amplitude. Migration selectively suppresses frequencies too high for penetration at the given depth, and preserves the frequencies that can penetrate to this depth. The suppression makes migration stable in the presense of high frequency noise, but limits the resolution. Analogous to the seismic case, the ratio of the backward propagated scattered electromagnetic field and the primary field is proportional to the reflectivity

coefficient at a geoelectrical boundary. This property is used to image geoelectrical structures.

Thus, formulating the electromagnetic migration problem as a backward propagation of the diffusive field in reverse time, we need to solve numerically a boundary value problem for the diffusion equation. This could be done, for example, using a finite-difference approach. This approach is attractive because it allows us to backward propagate the field through inhomogeneous media. We, however, have chosen a simpler approach, which is based on Green's theorem. According to Green's theorem, the field at any point inside some domain could be expressed via the values of the field at the domain's boundaries. Approximating the earth surface by the plane and considering the lower half-space as a domain for analytic continuation, one can express the value of the backward propagating field at any time moment at any particular depth via an electromagnetic analog of the Rayleigh integral. This integral has the same form as the well-known seismic Rayleigh integral, the only difference being that instead of the wave equation Green's function we use the diffusion equation Green's function, expressed in reverse time.

Thus, the backward propagated field focuses the secondary field on the boundary of a scatterer. At this point, the migrated field should be transformed into a resistivity image of the resistivity ingomogeneity. The key step in such a transformation is estimation of the incident field, because the ratio of the incident and the scattered field gives the reflectivity function, which could be recomputed to give the anomalous resistivity.

It is possible numerically to downward continue the primary field from the surface to the lower half-space. However, for the sake of simplicity, in this work we approximate the primary field by the plane wave propagating in a homogeneous medium. This approach allows us to analytically estimate the primary field at every point in the lower half-space at the zero time moment, thus providing a simple algorithm which transforms the amplitudes of the migrated field to *the migration apparent resistivity.*

Based on this theory, the computer code was created. The code consists of two major parts. The first part of the code takes the values of the field component on

the surface and computes the migrated field at zero time moment at every point of space, using a Rayleigh-type integral. This part of the code was tested by comparing the analytic solution for the plane wave in a two-layered model with the numerical solution.

The second part of the code takes values of the horizontal component of electric field at the zero time moment in the lower half-space and computes the migration apparent resistivity, approximating the primary field by the plane wave. The whole code is tested on 2D numerical models. The stability and resolution of the EM migration procedure are illustrated by the results of numerical modeling.

1.3 Waste site characterization

EM migration was applied to the interpretation of a TDEM data set acquired at the Cold Test Pit site within the Radioactive Waste Management Complex (RWMC) at the Idaho National Engineering Laboratory (INEL) (MacLean, 1993).

The Cold Test Pit was specifically constructed to investigate the ability of TDEM systems to characterize DOE nuclear waste sites. The prime goal of the geophysical survey at the Pit was to locate conductive drums, simulating nuclear waste containers.

The containers were buried at known places in the Pit. The data were obtained as a result of a high density TDEM profiling survey with the Geonics EM47 along the set of profiles, intersecting the Cold Test Pit. As a result a large volume of TDEM data were acquired.

TDEM migration was employed to process and interpret the 3D TDEM data. TDEM migration and resistivity imaging made it possible to outline the boundaries of the Cold Test Pit and characterize the distribution of the anomalous conductivity, thus directly pointing to the location of the drums. Migration results were compared with "smoke ring" imaging, which was done on the same data. "Smoke ring" imaging failed to resolve separate conductive bodies, but provided a reasonable estimation of the background resistivity. In contrast, migration apparent resistivity maps indicate not only the thickness of capping but also the depth extent of the Pit.

2. THEORY OF EM MIGRATION

In this section the theory of the EM migration method is considered. The following three subsections deal with the mathematical formulation of the migration problem, the extremal properties of the migrated field and estimation of the anomalous conductivity using the migrated field. The last two subsections outline important theoretical aspects of algorithm realization and describe the analytic solution which was used to test the code.

2.1 Downward continuation in reverse time

Consider a model in which the horizontal plane, $z = 0$, separates the conductive earth ($z > 0$) from the insulating atmosphere ($z < 0$). The conductivity in the earth, $\sigma(\vec{r})$, is represented as the superposition of a constant normal (background) conductivity, $\sigma_n = const$, and an anomalous conductivity function, $\Delta\sigma(\vec{r})$ (Berdichevsky and Zhdanov, 1984):

$$\sigma(\vec{r}) = \sigma_n + \Delta\sigma(\vec{r}). \tag{1}$$

Everywhere in the earth outside the anomalous region, the electromagnetic field satisfies the diffusion equation:

$$\Delta\vec{H} - \mu_0\sigma_n\frac{\partial\vec{H}}{\partial t} = 0, \quad \Delta\vec{E} - \mu_0\sigma_n\frac{\partial\vec{E}}{\partial t} = 0. \tag{2}$$

For this model, we can discuss the problem of migration of any scalar component, $P(\vec{r}, t)$, of an observed electromagnetic field.

Let us define *the migrated field,* P^m, obtained from a specific scalar component, P^0, of the electromagnetic field observed at the earth's surface as being the field that satisfies the following conditions:

$$P^m(\vec{r},\tau)\mid_{z=0}=\begin{cases} P^0(r,T-\tau)_{z=0} & \text{for } 0\le\tau\le T, \\ 0 & \text{for } \tau<0,\ \tau>T \end{cases} \tag{3}$$

$$\Delta P^m(\vec{r},\tau)-\mu_0\sigma\frac{\partial P^m(\vec{r},\tau)}{\partial\tau}=0 \text{ for } z>0, \tag{4}$$

and

$$P^m(\vec{r},\tau)\to 0, \tag{5}$$

for $\mid\vec{r}\mid\to\infty$, $\dot{z}>0$, where $\tau=T-t$ is reverse time, and T is the interval of electromagnetic signal recording.

Note that if we exchange the reverse time, τ, for ordinary time, t, in eq. (4), we have an equation which is the adjoint to the diffusion equation:

$$\Delta P^m(\vec{r},t)+\mu_0\sigma\frac{\partial P^m(\vec{r},t)}{\partial t}=0. \tag{6}$$

If the ordinary diffusion equation describes field propagation from the sources to receivers, then eq. (6) describes the inverse process of propagation from receivers to sources.

The problem of establishing the migrated field reduces to the downward extrapolation of the field P^0 from the earth's surface into the lower half-space in the reverse time, τ. This procedure is called *electromagnetic field migration* (Zhdanov and Frenkel, 1983; Zhdanov and Keller, 1994).

It can be seen from these considerations that the calculation of a migrated field is reduced to a boundary value problem described by eqs. (3) through (5). This boundary value problem can be solved using Green's theorem and the Green's function G for the 3D diffusion equation (Morse and Feshbach, 1953):

$$G(r',t'\mid r,t)=-\frac{(\mu_0\sigma)^{1/2}}{8\pi^{3/2}(t'-t)^{3/2}}e^{-\mu_0\sigma|r'-r|^2/4(t'-t)}H(t'-t), \tag{7}$$

which satisfies the equation:

$$\Delta G + \mu_0 \sigma \frac{\partial G}{\partial t} = \delta(\vec{r} - \vec{r}')\delta(t - t'). \tag{8}$$

Here $H(t' - t)$ is a Heaviside excitation function (step-function):

$$H(t - t') = \begin{cases} 0; & t' - t < 0 \\ 1; & t' - t > 0. \end{cases}$$

The problem of downward continuation of the field P (the field observed on the surface) can be solved using equation (6) (Zhdanov and Keller, 1994). Let us denote the lower half-space as D, and the surface of the earth as S. Introducing a hemisphere O of large radius R we can construct a closed contour $S + O$ around the domain D. Multiply the the left and right sides of equation (6) by G and integrate both sides over the infinite time range and over the space domain D. We then transform the volume integral over D to a surface integral over $S + O$ using Green's formula and taking equation (6) into consideration. Thus we have

$$P^m(\vec{r}', t') = \int_{-\infty}^{\infty} \int_{S+O} \left(P \frac{\partial G}{\partial n} - G \frac{\partial P}{\partial n} \right) ds dt, \tag{9}$$

for all r' inside domain D. The same equation remains valid if we replace G with the sum $(G + g)$, where g is an arbitrary solution to the homogeneous diffusion equation in D

$$P^m(\vec{r}', t') = \int_{-\infty}^{\infty} \int_{S+O} \left(P \frac{\partial (G + g)}{\partial n} - (G + g) \frac{\partial P}{\partial n} \right) ds dt.$$

Assume that the auxilary field g goes to zero as R goes to infinity. The S is the surface of observations, thus the normal derivative is equal to vertical derivative, so

$$P^m(\vec{r}', t') = \int_0^T \int_{-\infty}^{\infty} \left(P \frac{\partial (G + g)}{\partial z} - (G + g) \frac{\partial P}{\partial z} \right) ds dt. \tag{10}$$

If we take g as

$$g = -G(\vec{r}' - \vec{r}'', t),$$

where the point r'' is located symmetrically to r' with respect to the plane $z = 0$. Then

$$G + g = 0 \quad ; \quad \frac{\partial(G+g)}{\partial z} = 2\frac{\partial G}{\partial z}, \text{ for } z = 0. \tag{11}$$

Substituting equations (11) in equation (10), and after some algebraic operations we have the following representation for the migrated field:

$$P^m(\vec{r}', T - t') = 2\int_{t'}^{T}\int_{-\infty}^{\infty} P(\vec{r}, t)\frac{\partial \tilde{G}(\vec{r}', t' \mid \vec{r}, \tau)}{\partial z} dx dy dt, \tag{12}$$

where $\tilde{G}$ is the adjoint to the Green's function G for the diffusion equation (Morse and Feshbach, 1953; Zhdanov et al., 1988). The vector $\vec{r}\,'$ represents the image point of the migration field, and the vector $\vec{r}$ represents the integration point on the surface.

Equation (12) is the electromagnetic counterpart to the Rayleigh integral (Schneider, 1978; Claerbout, 1985). Just as in the seismic application, eq. (12) defines in space and normal time a field propagating towards the surface of observation (that is, upgoing waves), as can be seen from the fact that eq. (12) contains the function $\tilde{G}$, adjoint to the Green's function G of the diffusion equation. Hence, just as in the seismic case, a migration transformation of the electromagnetic field yields the upgoing field.

Let us consider the special case of the 2D model of the electromagnetic field (for example the E polarized mode) and a profile observation. We assume that the axis X coincides with the profile, and axis Y is orthogonal to the profile of observations. In this case the expressions for the different components of the migrated magnetic field, $H^0_{x,z}(x, 0, t)$, observed along the profile X on the surface of the earth, will have the form:

$$H^m_{x,z}(x', z', T - t') = \frac{\mu_0 \sigma_n z'}{4\pi}\int_{t'}^{T}\int_{X} H^0_{x,z}(x, 0, t)\frac{1}{(t - t')^2}\times$$

$$\times \exp\left\{-\frac{\mu_0 \sigma_n}{4(t - t')}\left[(x' - x)^2 + (z' - z)^2\right]\right\} dx dt, \tag{13}$$

and analogously for the electric field:

$$E_y^m(x', z', T - t') = \frac{\mu_0 \sigma_n z'}{4\pi} \int_{t'}^{T} \int_X E_y^0(x, 0, t) \frac{1}{(t - t')^2} \times$$

$$\times \exp\left\{ -\frac{\mu_0 \sigma_n}{4(t - t')} \left[(x' - x)^2 + (z' - z)^2 \right] \right\} dx dt. \tag{14}$$

Note, that typical EM equipment uses receiver loops for measuring the components of the magnetic field. Therefore, the actual data are proportional to the time-derivative of the magnetic field variations $\frac{\partial}{\partial t} H_{x,z}^0(x, 0, t)$. Thus we have to modify (13):

$$\frac{\partial}{\partial t'} H_{x,z}^m(x', z', T - t') = \frac{\mu_0 \sigma_n z'}{4\pi} \int_{t'}^{T} \int_X \frac{\partial}{\partial t} H_{x,z}^0(x, 0, t) \frac{1}{(t - t')} \times$$

$$\times \exp\left\{ -\frac{\mu_0 \sigma_n}{4(t - t')} \left[(x' - x)^2 + (z' - z)^2 \right] \right\} dx dt. \tag{15}$$

The last expression gives a possibility in the 2D case of calculating the migrated electric field from the observed vertical component of the magnetic field, since from the second Maxwell's equation for the migrated field we have:

$$\frac{\partial E_y^m}{\partial x} = -\mu_0 \frac{\partial H_z^m}{\partial \tau},$$

and

$$E_y^m(\tilde{x}, z', T - t') = \mu_0 \int_{x_L}^{\tilde{x}} \frac{\partial}{\partial t'} H_z^m(x', z', T - t') dx', \tag{16}$$

where $(\tilde{x}, z')$ is a current point of electrical field calculations, and x_L is a horizontal coordinate of the left end point on the profile.

Thus, from the observed vertical component of the magnetic field we can calculate the migrated magnetic field at any level z' and then determine the migrated electric field E_y^m at the same level.

In a TDEM sounding one typically measures the electromagnetic response of a

step-function current waveform. However we will see below that for migration imaging it is important to have a capability of converting these data into the delta-pulse current response. The conversion of electromagnetic measurements due to a step-function current to that due to delta-pulse current can be done in the process of migration.

The delta-pulse response can be obtained from the step-pulse response by differentiation with respect to time. Therefore we can use equation (15) and after integration by parts obtain the time derivative of the migration field, which is equal to the migrated step response electrical field:

$$H_{x,z}^{m\delta}(x',z',T-t') = \frac{\partial}{\partial t'} H_{x,z}^{mstep}(x',z',T-t') =$$

$$\frac{\mu_0\sigma_n z'}{16\pi}\int_{t'}^{T}\int_X H_{x,z}^{step}(x,0,t)\frac{-8(t-t')+\mu_0\sigma_n\left[(x'-x)^2+(z'-z)^2\right]}{(t-t')^4}\times \tag{17}$$

$$\times\exp\left\{-\frac{\mu_0\sigma_n}{4(t-t')}\left[(x'-x)^2+(z'-z)^2\right]\right\}dxdt,$$

where $H_{x,z}^{step}$ are step-function responses and $H_{x,z}^{m\delta}$ are migrated delta-pulse responses.

2.2 Resistivity imaging by TDEM migration

At this point we will give a description of the basic concepts in which migration imaging of geoelectric structures is based.

To illustrate the "EM radiating-inhomogeneities" concept, we represent the observed electromagnetic fields $\vec{E}$, $\vec{H}$ as being the sum of a primary field, $\vec{E}^p, \vec{H}^p$, and a secondary field, $\vec{E}^s, \vec{H}^s$:

$$\vec{E} = \vec{E}^p + \vec{E}^s,$$

$$\vec{H} = \vec{H}^p + \vec{H}^s, \tag{18}$$

where the primary field is defined as being that field which is generated by a specific source in the earth with the normal distribution of the electrical conductivity $\sigma_n(r)$ (say, in a homogeneous half-space) and the secondary field is due to the anomalous conductivity distribution. In other words we can treat the secondary field as

the field generated by the extrinsic (anomalous) currents concentrated in localized inhomogeneous domains.

The fact that the integral formula (12) contains the adjoint Green's function for the diffusion equation means that, as in the wave case, a field determined in the space by these integrals represents an assembly of electromagnetic "waves" moving towards the observation surface. However, in view of the specifics of the diffusion equation, this field does not feature such simple and effective geometrical properties as the Claerbout upgoing wave, which ensures a direct reconstruction of reflection boundaries by the location of backpropageted wavefront at the instant $t' = 0$. We will see nevertheless that the migration electromagnetic field also can be used for detecting local inhomogeneities in a conducting medium, and for determination of geoelectrical boundaries.

To simplify our discussion we assume that the secondary field is generated by the delta-pulse currents switching on at zero time. This field propagates in different directions, and is observed on the surface of the earth. The idea of electromagnetic migration consists of reverse downward extrapolation of the observed field in reverse time. When the time reaches zero, the extrapolated field is at the location of the scatterer. Thus, in the case of the secondary field this downward extrapolation in reverse time will result in the focusing of the migrated field at zero time at the location of the source.

Note that in reality the behavior of the sources of the secondary field is more complicated than the delta pulse. Since the propagation is dispersive, these sources "switch on" instantaneously, and the field builds up to the maximum with some delay, related to the time of propagating the primary field from the earth's surface to the geoelectrical inhomogeneties. That is why we have two options: 1) to reconstruct the migration field in the lower halfspace not at zero time, but at a retarded time, or 2) to use for the downward extrapolation not the actual background conductivity, but instead some effective *migration conductivity* σ_m proportional in the general case to the normal conductivity $\sigma_m = \gamma\sigma_n$, where γ is called the *migration constant.* Detailed analysis of geoelectrical models shows that in the second case we can select the

migration conductivity σ_m in such a way that the extremum of the migration field at zero time coincides with the geoelectrical boundaries. Using the migration conductivity instead of the background conductivity allows us to keep the traditional imaging conditions, namely to construct the image as a function of the migration secondary field at zero time moment. It is shown in the Appendix A that such an imaging condition is correct for the earth with slow horizontal variations of conductivity and plane wave excitation. In the Appendix B the migration apparent resistivity concept is discussed. The migration procedure is used to focus the field at the anomalous structure, then the analytic formula for the two-layered model and the quasi-plane wave exitation is used for an arbitrary earth model and an arbitrary source to image the conductivity structure.

Approximation of the source field by the plane wave is valid for two cases. The first case is the far-field of the fixed transmitter (Zhdanov and Keller, 1994). The source's far field consists of the part propagating through the air and the part propagating through a conductive earth. The air field can be approximated by the plane wave because it arrives at every point simultaneously, and the part propagating through the ground can be neglected because it attenuates in the conductive earth (see Figure 1a.)

The second case is a slingram mode survey design. For the slingram mode we can use an analogy with seismic migration. As it is shown by Claerbout (1972), suming up records from many receivers (homogeneusly distributed along the profile) one can obtain a single record corresponding to a plane wave incident field. The primary field propagation for this case is shown in Figure 1b.

To illustrate the focusing properties of the migration, we migrate the field generated by an infinitely long conductive cable. The electrical field excited on the surface by the buried electrical cable could be computed using the Green's function of the diffusion equation G, which is given by formula (7). The field of an electrical cable on the surface is presented in Figure 2. The background resistivity is 100 Ωm and the cable depth is 100 m.

The result of migration is shown in Figure 3. It indicates that the migrated field

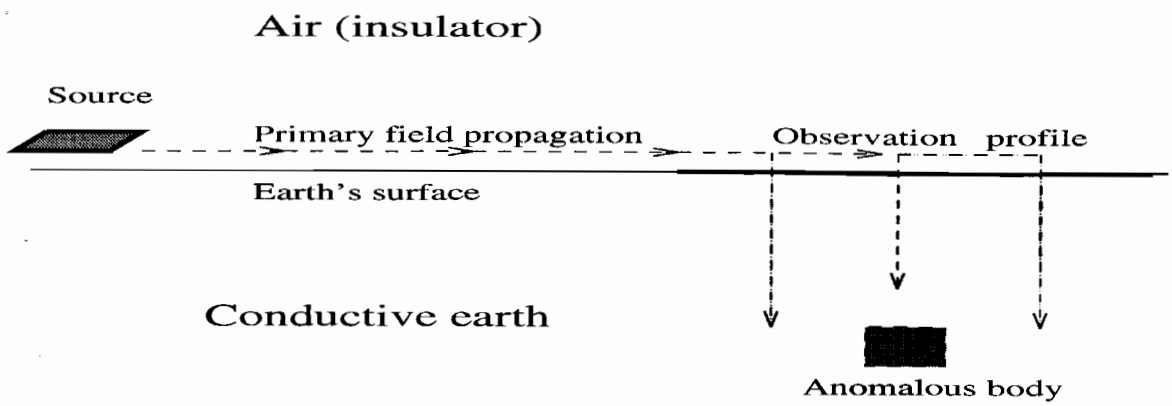

a)

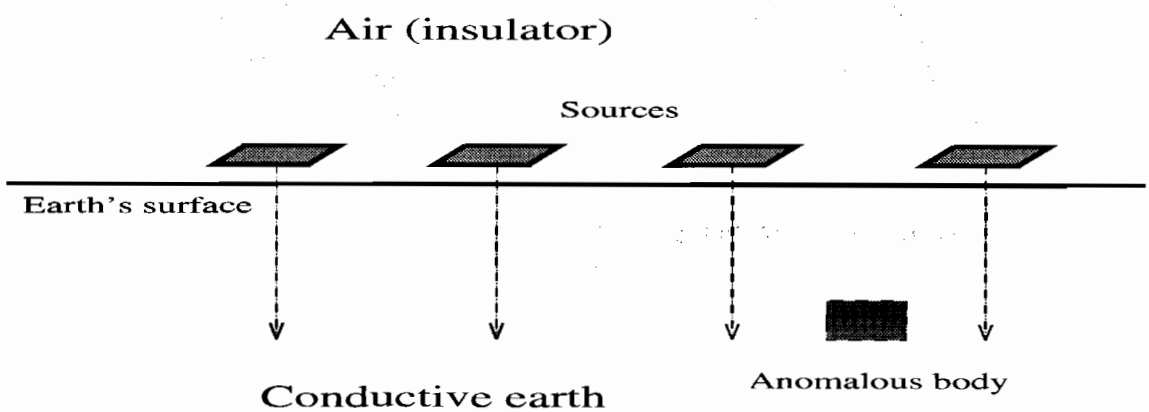

b)

Figure 1: Approximation of the primary field propagation by the plane wave. a) Primary field propagation in the far zone. b) Primary field in slingram mode.

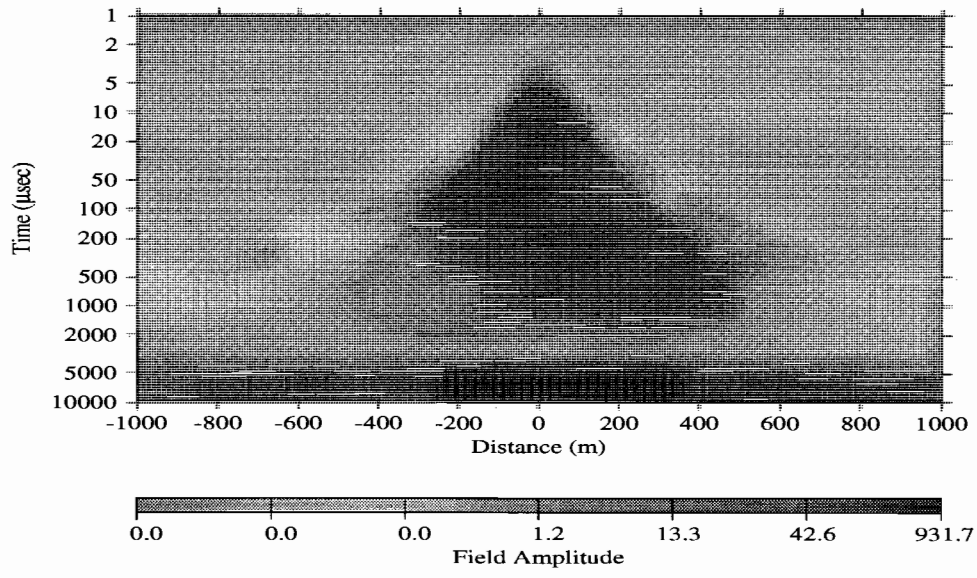

Figure 2: Surface response of an electrical field simulated for a buried cable.

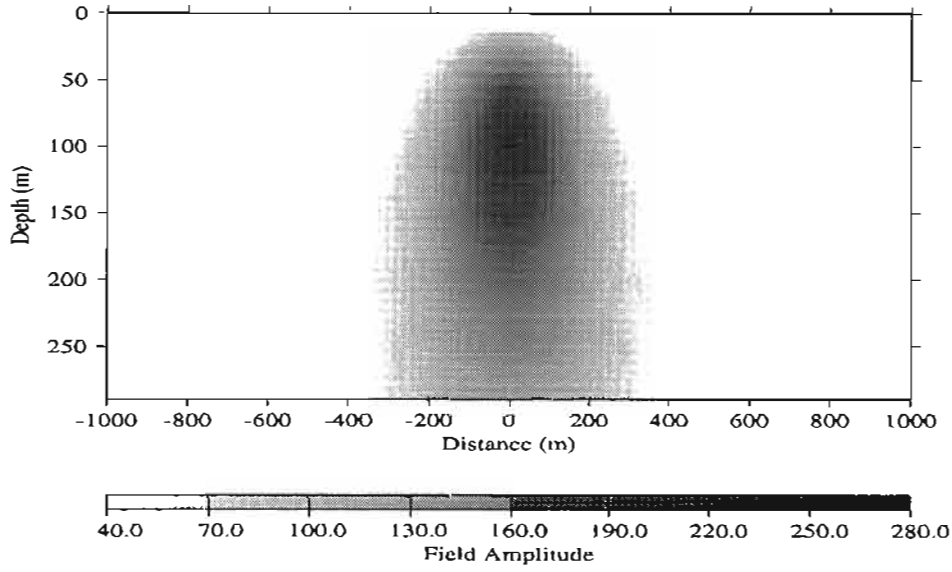

Figure 3: Migrated field of the electrical cable response. Cross shows the location of the cable.

has a maximum at the point of the cable location. This illustrates how the migrated field represents the location of a subsurface target. The actual field has a singular point at the source location, whereas the migration field has a maximum at the source location. In the real case where the subsurface inhomogeneous structure is excited by the field source located on the surface, the migration field still has a maximum at the point of an anomalous structure, which acts like a secondary source.

Furthermore, we develop the technique to transform the EM migration fields and their different components into resistivity images of the vertical cross-section.

It was shown in (Zhdanov and Booker, 1993; Zhdanov and Keller, 1994) that in the frequency domain for plane wave secondary (upgoing) and primary (downgoing) fields everywhere inside the conducting layer are characterized by different amplitudes and phases. On the geoelectric boundaries their phases coincide (or shifted by π), while the amplitude of the upgoing wave is proportional to the amplitude of the downgoing wave and the proportionality factor is equal to the reflectivity coefficient β. When passing into the time domain the above regularities manifest themselves in the fact that the time pulses of the upgoing and downgoing waves differ everywhere inside the conducting layer and mutually proportional to the coefficient β only at the geoelectric boundary (see Appendix A).

We can introduce a time domain apparent reflectivity function, $\beta_{ta}(\vec{r},t)$, defined as the ratio of the secondary $E_y^s(\vec{r},t)$ and primary $E_y^p(\vec{r},t)$ fields, as the following:

$$\beta_{ta}(\vec{r},t) = E_y^s(\vec{r},t)/E_y^p(\vec{r},t). \tag{19}$$

The determination of this function, obviously, depends upon the procedure for downward extrapolating upgoing and downgoing fields in the lower half space. However, it can be generalized to the results of time-domain electromagnetic migration.

In Appendix A we show that the migration apparent reflectivity function at zero time, $\beta_a^m(\vec{r})$, can be determined also from the values of the migrated secondary field, calculated at zero time and normalized by some function $D(\vec{r})$,

$$\beta_a^m(\vec{r}) = E_y^{ms}(\vec{r},0)/D(\vec{r}), \tag{20}$$

where $D(\vec{r})$ is the convolution of the migrated primary field at the same depth and the analytical function $\varphi(z,\tilde{t})$

$$D(\vec{r}) = D(x,z) = \int_0^{+\infty} H_z^{mp}(x,z,t)\varphi(z,t)\,dt, \tag{21}$$

where

$$\varphi(z,t) = a\frac{z}{\tau^3}\exp\left[-2\pi^2\left(\frac{z}{\tau}\right)^2\right]. \tag{22}$$

In the last equation:

$$a = \frac{2^{7/2}\pi^{5/2}}{\mu\sigma_n} \text{ and } \tau = 2\pi\sqrt{2t/\mu\sigma_n}. \tag{23}$$

The function β_a^m is equal to the actual reflectivity coefficient β exactly at the position of the boundary:

$$\beta_a^m(\vec{r}) = \beta. \tag{24}$$

This result is based on the fact that the migrated secondary (upgoing) field has a local extremum exactly at the geoelectric boundaries. This extremum is proportional to the reflectivity of the boundary and to the magnitude of the downgoing (primary) field at the same point.

The reflectivity coefficient is connected with the conductivity contrast $\Delta\sigma$ at the geoelectrical boundary by the simple formula (see Appendix A):

$$\beta = \frac{\sqrt{\sigma_n} - \sqrt{\sigma_n + \Delta\sigma}}{\sqrt{\sigma_n} + \sqrt{\sigma_n + \Delta\sigma}}.$$

From the last formula we can determine the resistivity below the geoelectrical boundary (within the anomalous domain or layer):

$$\rho = \left[\frac{1+\beta}{1-\beta}\right]^2 \rho_n, \tag{25}$$

where ρ_n is the background (normal) resistivity. The last expression gives the exact value of the resistivity of the second layer in a two-layered model (see Appendix A). However, we can use this expression for an arbitrary model to define *the migration apparent resistivity.*

So, the migration apparent resistivity ρ_m can be calculated using the formula (40) at any point of the profile. Since the migration apparent resistivity ρ_m is a function of depth, we obtain immediately the geoelectrical cross section.

The migrated secondary field in expression (48) (Appendix A) is calculated at zero time, which corresponds to the secondary field in the vicinity of the source. We can compare this situation with the time domain field, where the depth of the field penetration inside the earth is proportional to the square root of the time after the current pulse in the transmitter: for early times the field is concentrated in the near surface layers; for later times the field penetrates deeper in the earth. In the case of the migrated field at early times this field is in the vicinity of its sources - the geoelectrical boundaries. At later times this field propagates upward to the earth's surface. So at early time the migrated field behavior is determined only by the properties of the medium near the boundary between two layers. Therefore it is plausible that eq. (19) could be used for determining the conductivity contrast between these layers.

In the case of a multilayered cross section we can start from the first layer and determine the resistivity of the second layer, then find the conductivity contrast between the second and third layer and determine the resistivity of the third layer, etc. This layer by layer process opens the way for direct imaging of complex geoelectrical structures. In a model with a complex multilayered structure we can take as ρ_n an apparent resistivity of the earth $\rho_a(t)$ obtained by averaging along the observation profile. The formula connecting the time t with depth d for the apparent resistivity calculation is provided by the following approximate expression for the skin-depth (Zhdanov and Keller, 1994):

$$d \approx \sqrt{2t\rho_a(t)/\mu_0}. \tag{26}$$

Thus an inhomogeneous profile of the earth's resistivity can be approximated by an homogeneous model which is used as the background (normal) resistivity for the migration. We call this normal resistivity profile the mean resistivity model.

This approach is similar to the one used in seismic prospecting where the real velocity distribution is replaced by the mean velocity (Claerbout, 1985) Also, as in seismic prospecting, we can use recursive migration algorithms which are based on successive downward extrapolation from level to level with different background resistivities.

The algorithm described above has been coded. Sample computations using this code are presented in the next section.

2.3 Numerical realization of the migration algorithm

For numerical realization of the EM migration algorithm, equations (15) and (17) must be reformulated in a discrete sense. These equations are essentially convolutions of the field observed on the surface with the Green's function or a derivative of the Green's function. Implementing these convolutions one can expect certain problems connected with the Green's function behavior. These problems are related to the fact that depending on the background conductivity value and migration depth, the Green's function and especially its time derivative can vary much faster than the observed field. Besides, in practice electromagnetic data are usually represented in logarithmic time, and the observed field is approximated by the average value within each specific interval or *time gate.*

So, rewriting time and spatial integrals in (15) over the whole integration domain as a sum of integrals over subdomains (time gates $\Delta t(i)$ and x-intervals $\Delta x(k)$) we have:

$$\frac{\partial}{\partial t'} H^m_{x,z}(x', z', T - t') = \frac{\mu_0 \sigma_m z'}{4\pi} \sum_{i=1}^{N_x} \sum_{k=1}^{N_t} \int_{\Delta t(i)} \int_{\Delta x(k)} \frac{\partial}{\partial t} H^0_{x,z}(x, 0, t) \frac{1}{(t - t')^2} \times$$

$$\times \exp\left\{-\frac{\mu_0\sigma_m}{4\,(t-t')}\left[(x'-x)^2+(z'-z)^2\right]\right\}dxdt.$$

We can express the second term as a time derivative, assuming that $H^0_{x,z}(x,0,t)$ is a step-response, to get

$$\frac{\partial}{\partial t'}H^m_{x,z}(x',z',T-t') = \frac{\mu_0\sigma_m z'}{4\pi}\sum_{i=1}^{N_x}\sum_{k=1}^{N_t}\int_{\Delta t(i)}\int_{\Delta x(k)} H^0_{x,z}(x,0,t)\times$$

$$\times\frac{\partial}{\partial t}\left(\frac{1}{(t-t')^2}\exp\left\{-\frac{\mu_0\sigma_m}{4\,(t-t')}\left[(x'-x)^2+(z'-z)^2\right]\right\}\right)dxdt.$$

Assuming that $H^0_{x,z}(x,0,t)$ is constant within each time gate $\Delta t(i)$ and each x-interval $\Delta x(k)$ we can take it out of the integral and after that calculate the integral over t of the time derivative of the Green's function. As a result we obtain a discrete form of the continuous convolution integral (15) as

$$\frac{\partial}{\partial t'}H^m_{x,z}(x',z',T-t') =$$

$$\sum_{i=1}^{N_x}\sum_{k=1}^{N_t}\left(H^0_{x,z}(x_i,0,t_i)\times G^m_o(x',x_k,x_{k+1},t_k,t_{k+1},t',z'-z)\right), \qquad (27)$$

where x_{k+1} and x_k are x-interval boundaries

$$\Delta x(k) = x_{k+1} - x_i,$$

and t_{i+1} and t_i are time gate boundaries

$$\Delta t(i) = t_{i+1} - t_i.$$

The function $G^m_o(x',x_k,x_{k+1},t_k,t_{k+1},t',z'-z)$ is called *the migration kernel*

$$G^m_o(x',x_k,x_{k+1},t_k,t_{k+1},t',z'-z) = \frac{\mu_0\sigma_m z'}{4\pi}\times$$

$$\times \int_{x_k}^{x_{k+1}} \frac{1}{(t_{i+1}-t')^2} \exp\left\{-\frac{\mu_0\sigma_m}{4\,(t_{i+1}-t')}\left[(x'-x)^2+(z'-z)^2\right]\right\} -$$

$$-\frac{1}{(t_i-t')^2} \exp\left\{-\frac{\mu_0\sigma_m}{4\,(t_i-t')}\left[(x'-x)^2+(z'-z)^2\right]\right\} dx. \qquad (28)$$

To obtain the formula for the delta-pulse excitation it is enough to replace the kernel (28) in the formula (27) by its time integral, (which could be calculated analytically)

$$G^m_{o1}(x', x_k, x_{k+1}, t_k, t_{k+1}, t', z'-z) = \int_{x_k}^{x_{k+1}} \frac{z'}{\pi((x'-x)^2+(z'-z))^2} \times$$

$$\times(\exp\left\{-\frac{\mu_0\sigma_m}{4\,(t_{i+1}-t')}\left[(x'-x)^2+(z'-z)^2\right]\right\} -$$

$$-\exp\left\{-\frac{\mu_0\sigma_m}{4\,(t_i-t')}\left[(x'-x)^2+(z'-z)^2\right]\right\})dx. \qquad (29)$$

The migration computer code is based on formulas (27) and (28). The code precomputes values of the migration kernel $G^m_o(x_k, x_{k+1}, t_k, t_{k+1}, t', z')$ for all sampling intervals $\Delta x(k)$ and $\Delta t(i)$ at particular depths z'. These values are stored as a matrix $G^m_o(i,k)$. Sampling over time and space should be chosen according to survey parameters. Then the migration program convolves matrices $G^m_o(i,k)$ with the matrix of magnetic field values $H^0_{x,z}(i,k)$, thus obtaining a migrated field at the depth z'. Repeating this procedure over all values z' one obtains a migrated field at each depth.

2.4 Testing of the algorithm

To check the accuracy of the migration algorithm we compared the secondary field in a two-layer earth model excited by a plane wave, migrated analytically and numerically. The analytical solution for the migration problem for a plane wave in a layer covering a homogeneous half-space is in Appendix A.

The E_y component of the secondary electric field for the model with one layer of

thickness h and conductivity σ_1 covering an infinite half-space with conductivity σ_2, excited by a plane wave with amplitude Q is expressed on the Earth's surface at any time moment t using the following formulas:

$$E_y^s(z=0,t) = Q\beta a \frac{2h}{\tau^3} exp(-2\pi^2(\frac{2h}{\tau})^2), \tag{30}$$

where variables a and τ are given by the expressions

$$a = \frac{2^{7/2}\pi^{5/2}}{\mu\sigma_1},$$

$$\tau = 2\pi\sqrt{2t/(\mu\sigma_1)},$$

and β is the reflectivity coefficient, which is given by the formula

$$\beta = \frac{\sqrt{\sigma_1} - \sqrt{\sigma_2}}{\sqrt{\sigma_1} + \sqrt{\sigma_2}}.$$

The migrated electrical field amplitude at any depth and at zero time moment can be expressed as

$$E_y^m(z, t=0) = \frac{-8Q\beta\sqrt{\sigma_1\sigma_m}hz}{\pi\mu(\sigma_1 4h^2 + \sigma_m z^2)^2}. \tag{31}$$

The parameters for the test are $\sigma_1 = 0.01\ S/m$, σ_2 =0.02 S/m, and $\sigma_m = 0.01333$ S/m. The first layer thickness is 100 m, and Q=0.05 V/m.

The secondary field, given by formula (30) and the migration kernel, both at z=0 are presented in Figure 4. Here the constant time discretization ($\Delta t = 1\mu s$) was used. We can see that the migration kernel changes with time much faster than the secondary field. This is the reason why we cannot directly discretize formula (15) for its numerical realization, applying instead the formula (27). Formula (27) uses the discrete migration kernel (27), which is an average value of the Green's function over each particular time gate.

The comparison of the analytical formula (31) with the migrated field computed

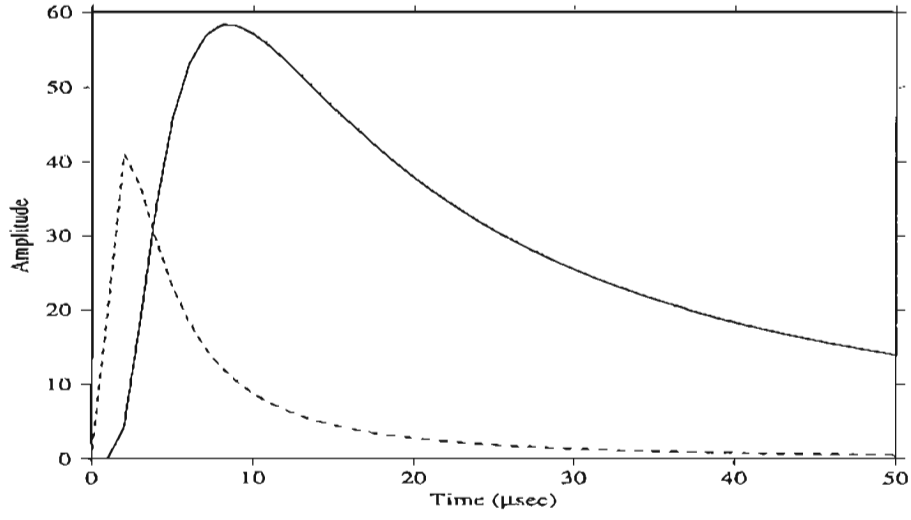

Figure 4: Secondary field for the model with one horizontal layer (solid line) and migration kernel (dashed line)

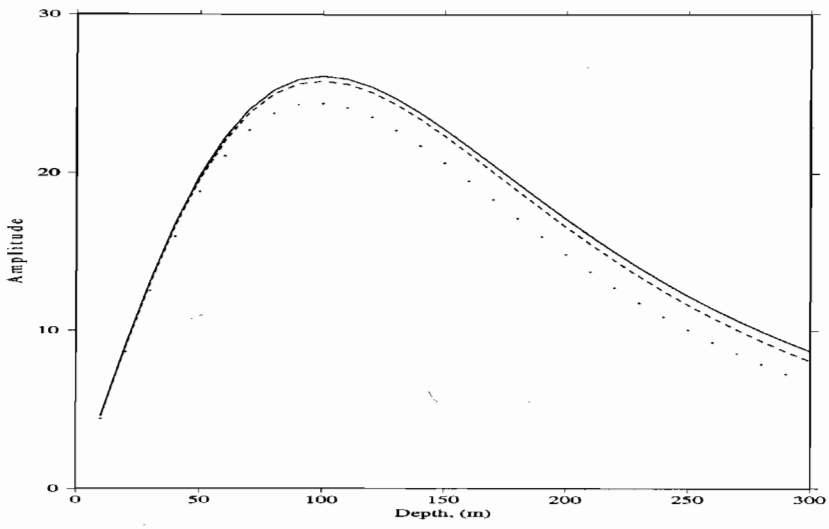

Figure 5: Analytic solution (solid line) and numerically migrated field. Aperture is 1000 m (dashed line) and 500 m (dots).

numerically for different apertures (see Figure 5) shows that the error in the algorithm is small and significantly decreases with increasing integration limits. For the numerical realization the time gates were chosen with 12 points per decade. Spatial sampling interval was equal to 40 m. The study has shown that the algorithm is sensitive to the spatial limits (aperture) of integration. To produce a reliable picture the limits of integration must be approximately 10 times wider than the depth of the target.

Figure 6 compares the migration results obtained for an aperture of 2000 m and grid spacings of 40 and 100 m. We can see that error decreases with decreasing spacing.

An empirical conclusion from this study is that spatial sampling interval must be less than half of the depth of the target to avoid significant integration errors.

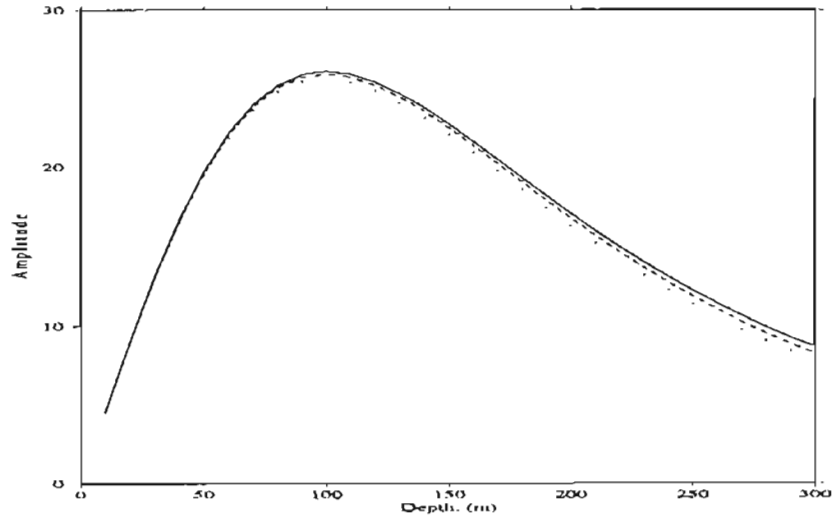

Figure 6: Analytic solution (solid line) and numerically migrated field. Grid spacing is 40 m (dashed line) and 100 m (dots).

3. MODEL STUDY

3.1 Modeling strategy and method

In this section the effectiveness of the TDEM migration method is analyzed for different geoelectrical models that can be considered typical for geophysical exploration and environmental studies.

The set of models under investigation includes: 1) models with local conductive bodies; and 2) models with local resistive and conductive bodies. These models simulate anomalous zones which are targets for geophysical surveys.

The theoretical survey in these models was conducted in the transmitter offset mode with fixed transmitter - receiver separation.

Time domain electromagnetic data are obtained as a result of forward modeling using computer code developed by J.I. Adhidjaja, G.W. Hohmann, and M.L. Oristaglio (1985). This code is based on the finite-difference method which gives a forward time domain solution for a 2D body in a conductive earth. This code is a reformulation of the TEM modeling method of Oristaglio and Hohmann (1984) in terms of the secondary field. The EM field in the models is generated by an infinitely long cable. The observed field is dH_z/dt and the transmitter-receiver separation (offset) is equal to 20 m. The cross-sectional dimensions of all anomalous bodies in the models (representing local inhomogeneities) are $20 \times 20\ m^2$.

The results of numerical modeling and TDEM migration demonstrate the effectiveness and stability for imaging different geophysical targets. We will demonstrate that TDEM migration is a fast and stable method of geoelectrical imaging, satisfactorily resolves the local inhomogeneities and gives a good estimate of the location, dimension and resistivity of the anomaly. The method, however, requires a good initial estimation of the background distribution of the conductivity. It is also based on the availability of the spatially dense measurements along the profile (2D) or over

a surface area (3D).

3.2 Model with one local conductive body

The steps of the migration can be illustrated using the following model. One local conductive body with resistivity 10 $Ohm - m$ is embedded in an homogeneous half-space with resistivity 100 $Ohm - m$. The vertical cross-section of the body is 20×20 m, while the depth to the body's top is 100 m (Figure 7). The numerical modelling code simulated a survey in slingram mode with a fixed 20 m transmitter/receiver separation, where the transmitter and receiver were moving together along the profile. It is assumed that the transmitter is excited by a step pulse and the receiver measures the time derivative of the magnetic field.

The modeling program produces a primary field which does not change along the profile (Figure 8). The time derivative of the secondary field, however, clearly indicates the spatial location of the anomaly (Figure 9). The migration procedure performed with a known background resistivity using formula (27) produces the *time derivative of the migrated magnetic field*, which is shown in Figure 10. Applying the transformation which is given by formula (16) one obtains the *migrated electrical field*, which is shown in Figure 11. This field indicates the depth of the anomalous body, as follows from the extremal properties of the migrated field. The estimated reflectivity function is shown in Figure 12. Using relationship (40), Appendix A, one finally arrives at the *migration apparent resistivity cross-section* (Figure 13), which could be viewed as a final result of the migration procedure. One can see that the migration apparent resistivity indicates the position and the resistivity of the conductive body.

3.3 The separation of primary and secondary field

An important problem arising in the practical realization of the migration algorithm is the separation of the secondary (scattered) field, i.e., the field associated with targets (scatterers), from the primary field. EM receivers measure the total field, which could be represented as a sum of the primary field (the field which is

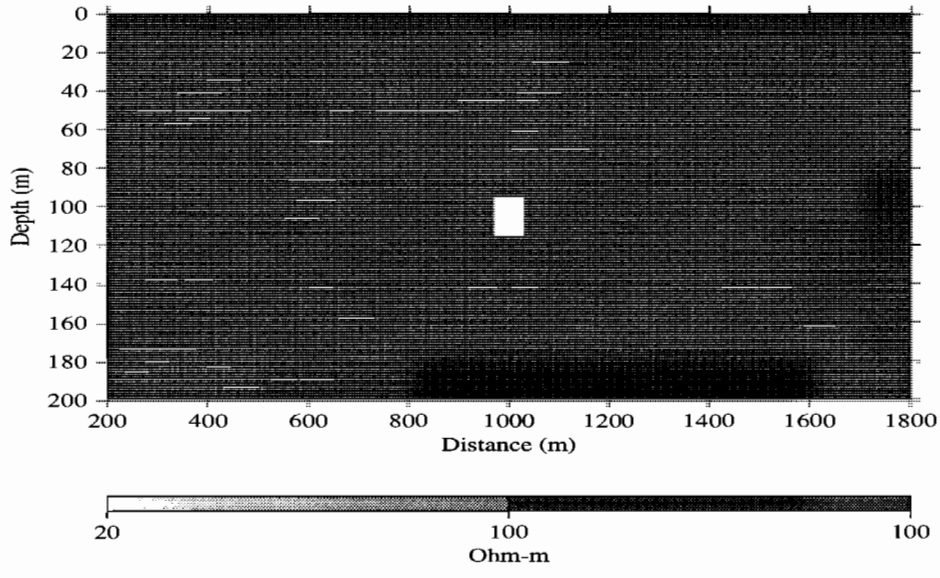

Figure 7: Local conductive body in a homogeneous media.

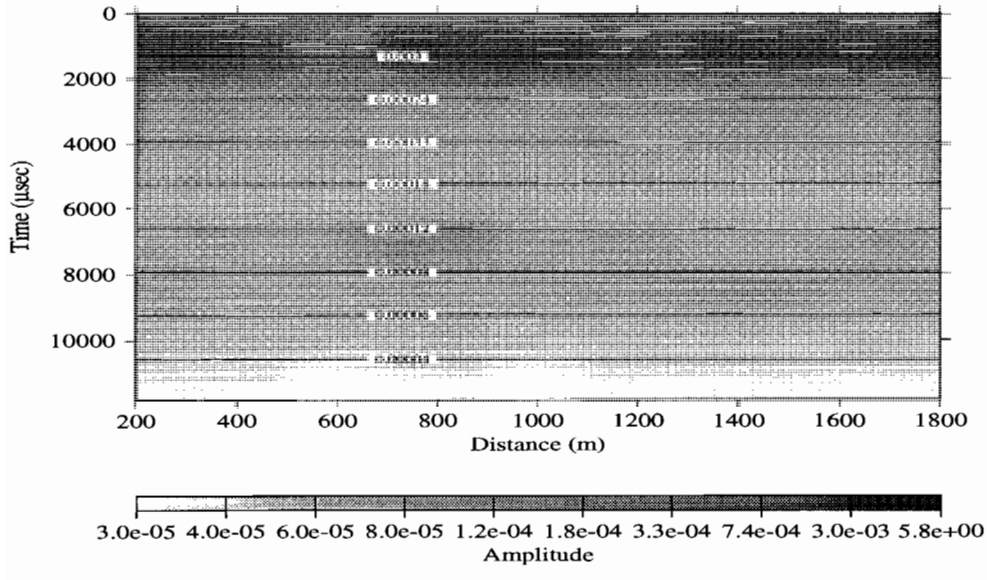

Figure 8: Time derivative of primary field for the model of Figure 7.

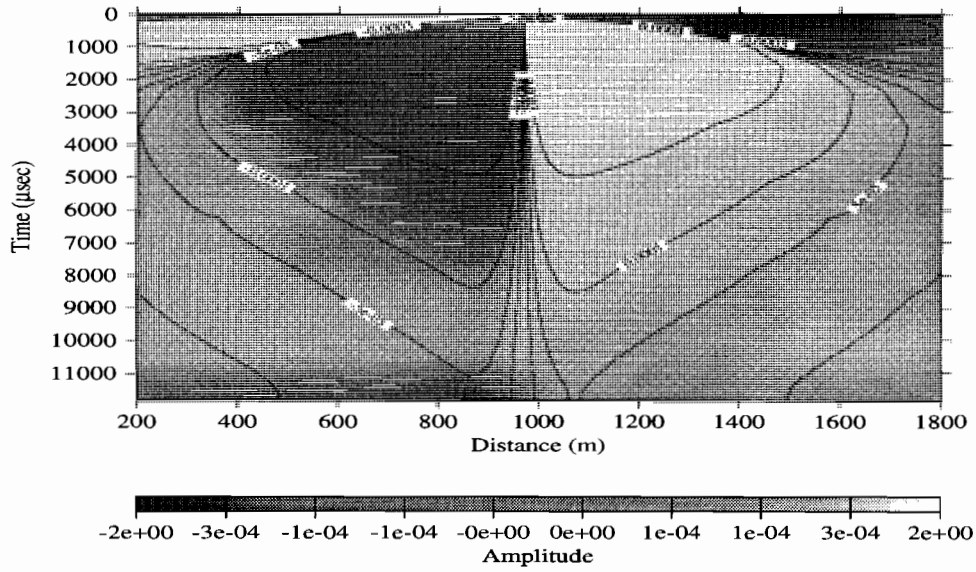

Figure 9: Time derivative of secondary field for the model of Figure 7.

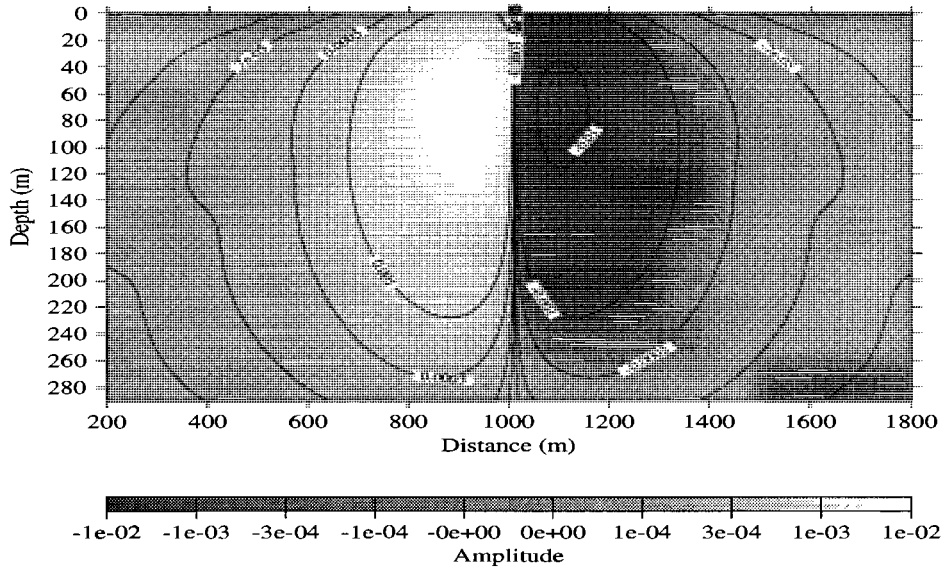

Figure 10: Migrated time derivative of magnetic field for the model of Figure 7.

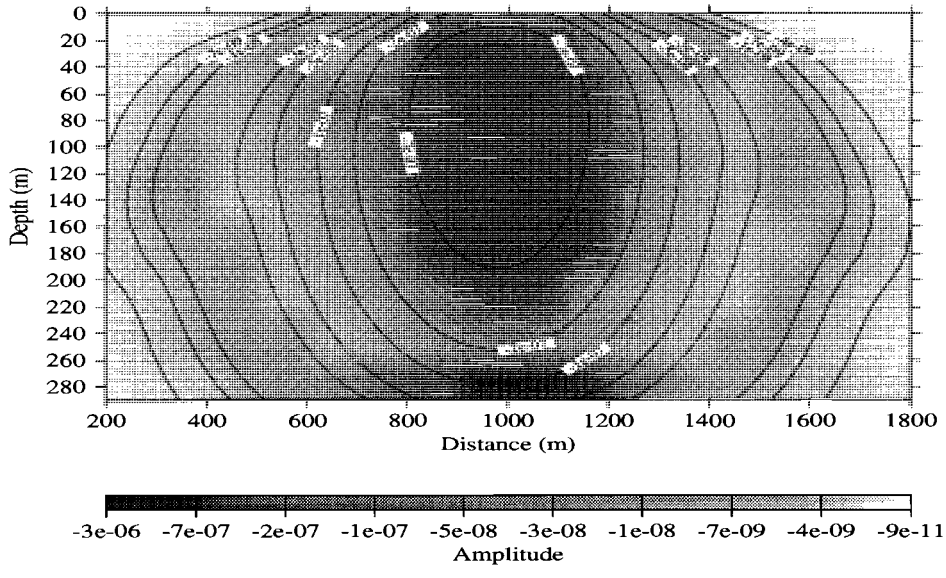

Figure 11: Migrated electric field for the model of Figure 7.

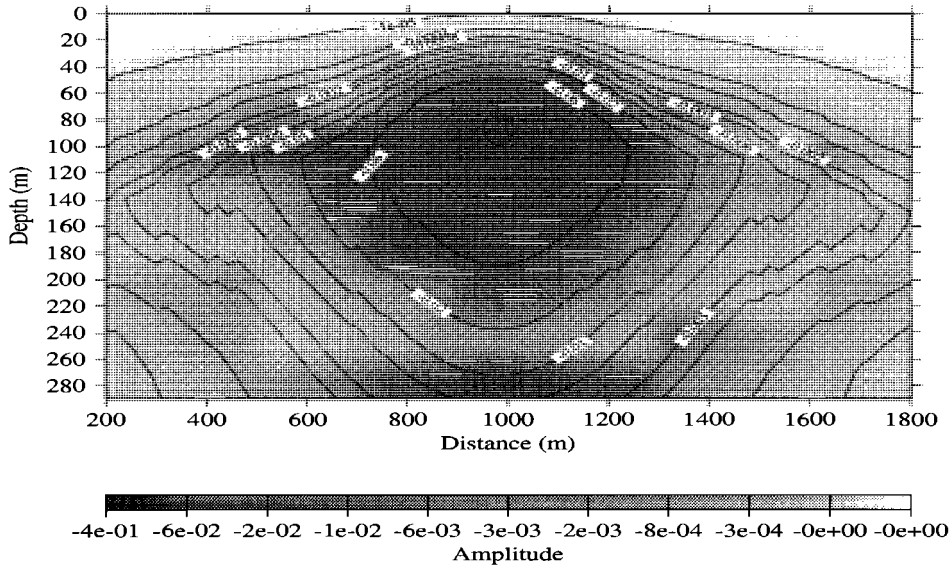

Figure 12: Apparent reflectivity function for the model of Figure 7.

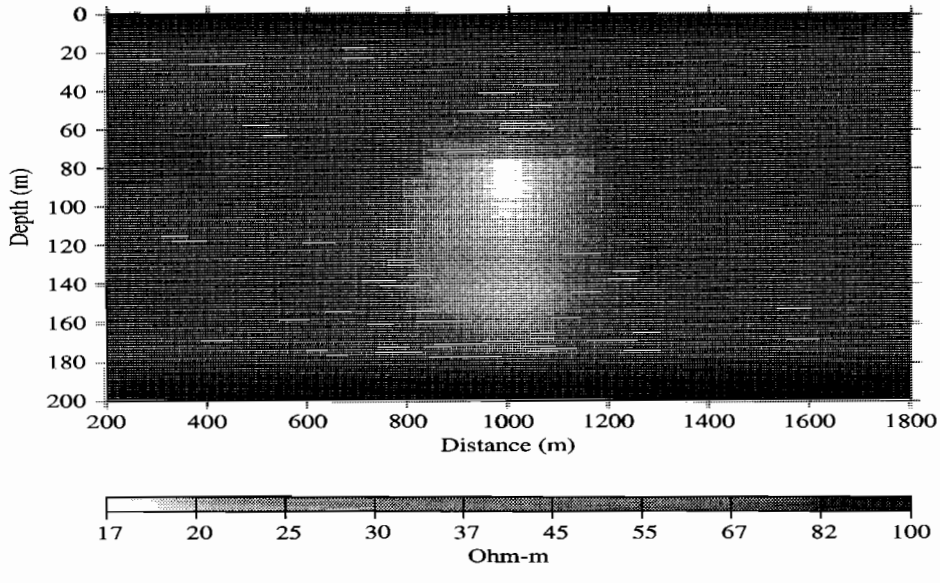

Figure 13: Migration apparent resistivity for the model of Figure 7.

observed in the absence of inhomogeneities), and the secondary field. In the case of slingram mode survey design and homogeneous media the primary and secondary field can be separated easily. We can see in Figure 8 that the primary field does not change along the profile. Figure 9 shows that the secondary field varies in both space and time. A plot of the secondary field values at 0.2 μsec versus X is shown in Figure 14. We can see from the plot that the area bounded by positive portions of the curve and the X-axis is equal to that bounded by the negative curve segments and the X axis. In Figure 14 we can see that the curve has mirror symmetry with respect to the point right above the anomalous body (X=0). We can understand the behavior of the primary and secondary fields by analyzing the model presented in Figure 15.

For a constant separation between transmitter and receiver, the primary field does not change as the system moves along the profile, since the geometric relationship between the source, the receiver and the horizontal layers do not change with respect to the source-receiver pair position.

However, the secondary field changes along the profile. Let us assume, for example, that the separation between the transmitter and receiver is small in comparison with the target depth. In this case, considering secondary fields we can assume the offset is zero. Now, consider two points X_1 and X_2, symmetrically located about the center of the body. The transmitter (in this case the infinite cable) located at the point X_1 produces an anomalous current in the body, with exactly the same direction and amplitude as if we place it at the symmetrical point X_2. The schematic vector lines of magnetic induction vector $\overline{B}$ are shown as dashed lines in Figure 15. The receiver (a small horizontal loop in this case) measures the inductive current which is proportional to the vertical component of magnetic field. We can see that vector lines at point X_1 are oriented upward, whereas at the point X_2 they are oriented downward. This means that the B_z components at the points X_1 and X_2 have opposite signs. But, because the geometry is symmetric, they have exactly the same amplitudes. Looking at Figure 15 we can conclude that the spatial spectrum of the anomalous magnetic field does not contain an harmonic with zero spatial frequency. In contrast, the spatial spectrum of the primary field contains only the zero frequency component.

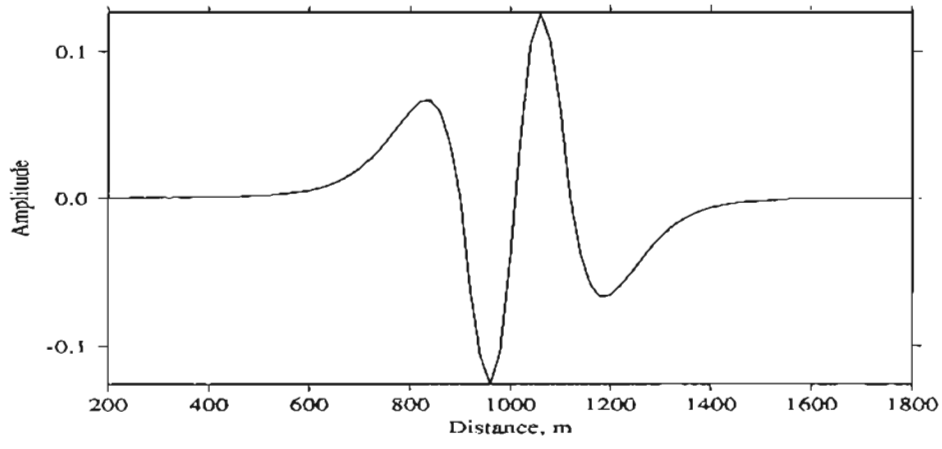

Figure 14: Secondary field at $0.2\mu s$.

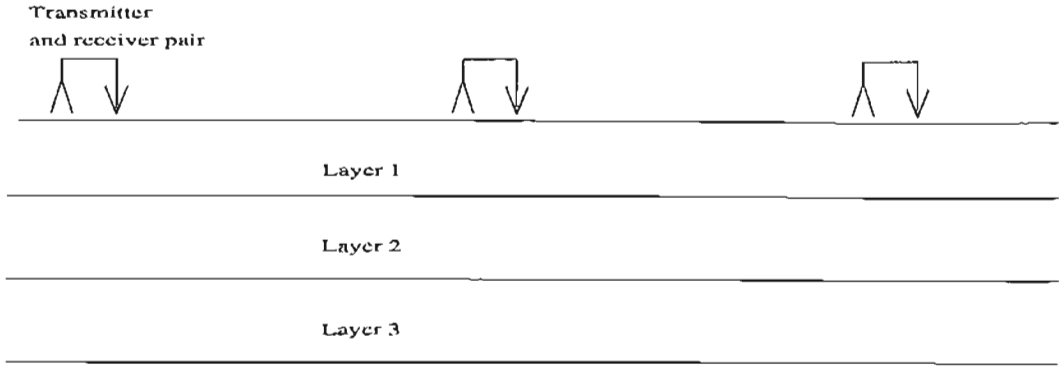

a)

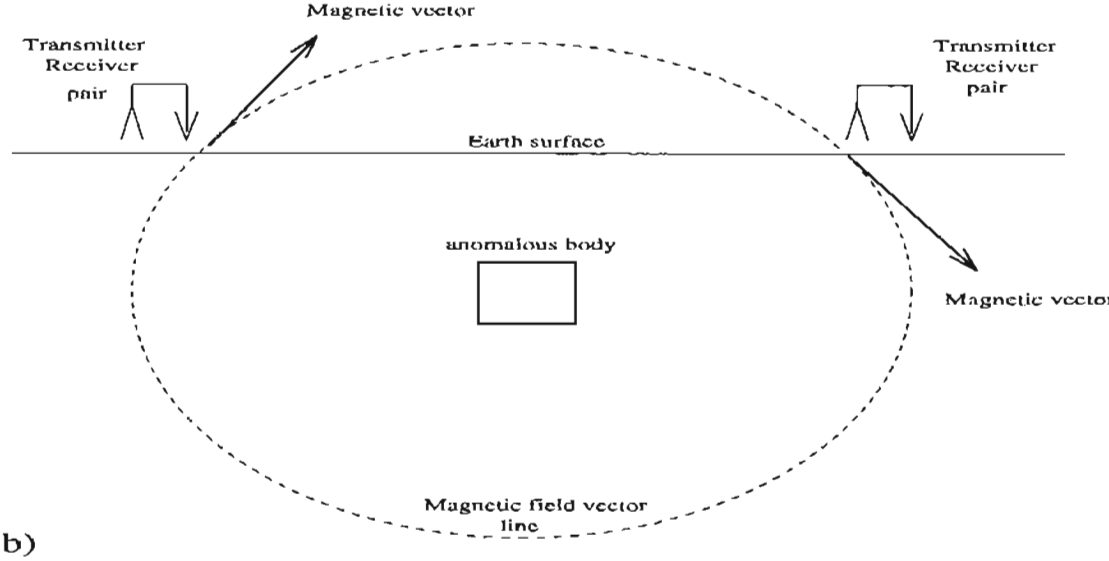

b)

Figure 15: Primary/secondary field separation. a) The primary field does not change along the profile above the horizontally layered media, b) secondary field is directed differently at symmetric points.

Thus, using spatial filtering, we can separate primary and secondary fields. This filtering can be realized by calculating the average value of the total field $\frac{\partial B_z^t(t)}{\partial t}$ along every time interval

$$\frac{\partial B_z^p(t)}{\partial t} = \frac{1}{Nx} \sum_{i=1}^{N_x} \frac{\partial B_z^t(t, x_i)}{\partial t},$$

where $\frac{\partial B_z^p(t)}{\partial t}$represents the primary field. The secondary field can be obtained for every point x_i using the formula

$$\frac{\partial B_z^s(t, x_i)}{\partial t} = \frac{\partial B_z^t(t, x_i)}{\partial t} - \frac{\partial B_z^p(t, x_i)}{\partial t}. \tag{32}$$

Formula (32) gives an exact solution for horizontally-layered media containing local inhomogeneous bodies. In spite of the fact that the real situation is more complex, application of spatial filtering for primary/secondary field separation has produced a reasonable result for the field data.

3.4 Migration of noisy data

In order to examine the effect of noise on the resolution of the migration method, we have added 5% random noise to the secondary field dH_z/dt computed on the Earth's surface. Figure 16 shows the same secondary field as in Figure 9, but with random noise added. The amplitude of the noise was distributed with constant probability between -5% and +5% of secondary field maximum.

Figure 17 represents the apparent resistivity image produced after the migration of this noisy secondary field. The migration resistivity image produced for the same model without adding noise is shown in Figure 13. As we can see, comparing the two pictures, the migration apparent resistivity calculated from the noisy data is very close to that calculated from the noiseless data. Similar results are obtained from the migration of noisy data for other models, discussed in the following sections.

This model illustrates the stability of the migration procedure for high-frequency random noise. This type of noise is typical for geophysical data. However, it does

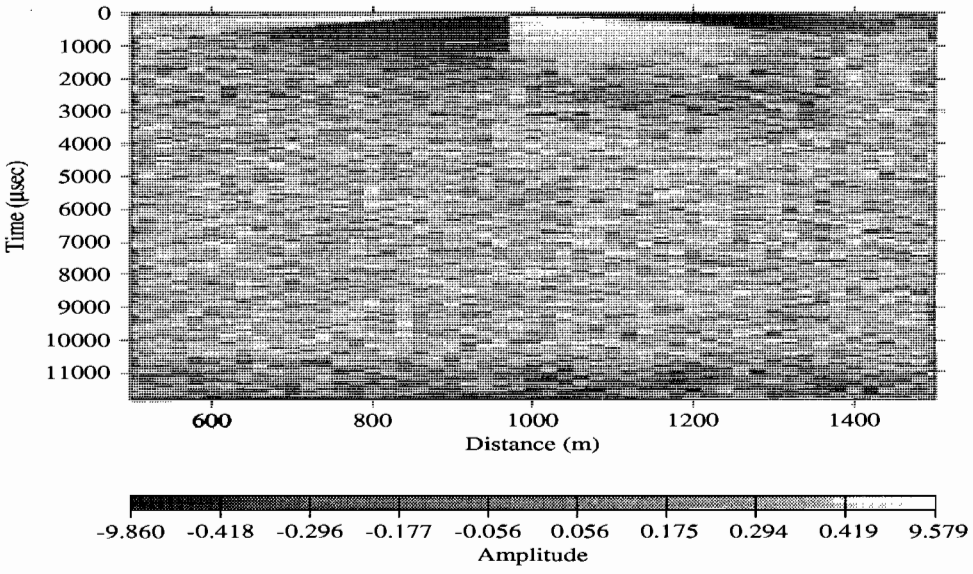

Figure 16: Secondary field with 5% random noise to field's maximum.

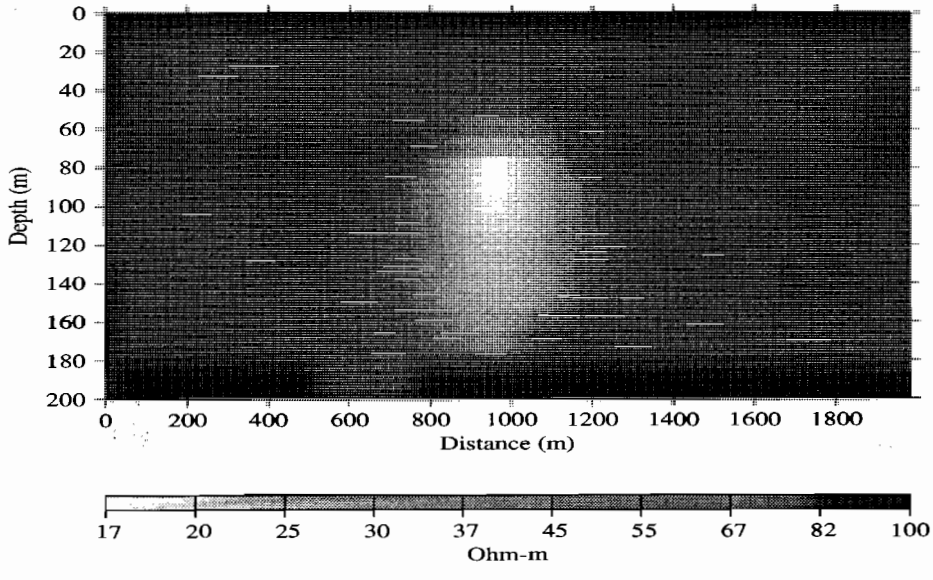

Figure 17: Migration image produced from noisy data.

not truly represent geological noise, produced for example, by near-surface inhomogeneities.

3.5 Resolution of migration method

In order to investigate the capability of migration method to resolve targets located close to each other, we compute a set of models with two conductive bodies, gradually changing the distance between the bodies.

The starting model consists of two conductive bodies with resistivity 20 Ohm-m and separation 100 m, embedded in an homogeneous medium of resistivity 100 Ohm-m at a depth of 100 m. Figure 18 shows the geoelectrical cross section of this model. Figure 19 shows that these two conductive bodies produce one single spot on the migration apparent resistivity image. Thus, for this separation, migration does not allow us to distinguish the two bodies separately.

The next model is similar to the previous one with the difference that the separation between the two conductive bodies is now increased to 200 m (Figure 20). The migration apparent resistivity image on Figure 21 shows that the two bodies can now be distinguished.

In the next model the separation between the two conductive bodies is increased to 300 m, as Figure 22 shows. The migration apparent resistivity image on Figure 23 demonstrates that for this separation the two bodies are very clearly distinguished and migration gives a good estimation of their location, resistivity and dimensions.

The analysis of these models suggests that for resolution of two conductive structures the distance between them should be at least two times greater than their depth.

3.6 Resolution of conductive and resistive bodies

It is known that a resistive body generally produces a much smaller anomaly than a conductive one. In order to demonstrate the capability of migration to distinguish a resistive body in the presence of a conductive body, we consider a model consisting of one conductive (20 Ohm-m) and one resistive (1000 Ohm-m) body embedded in a

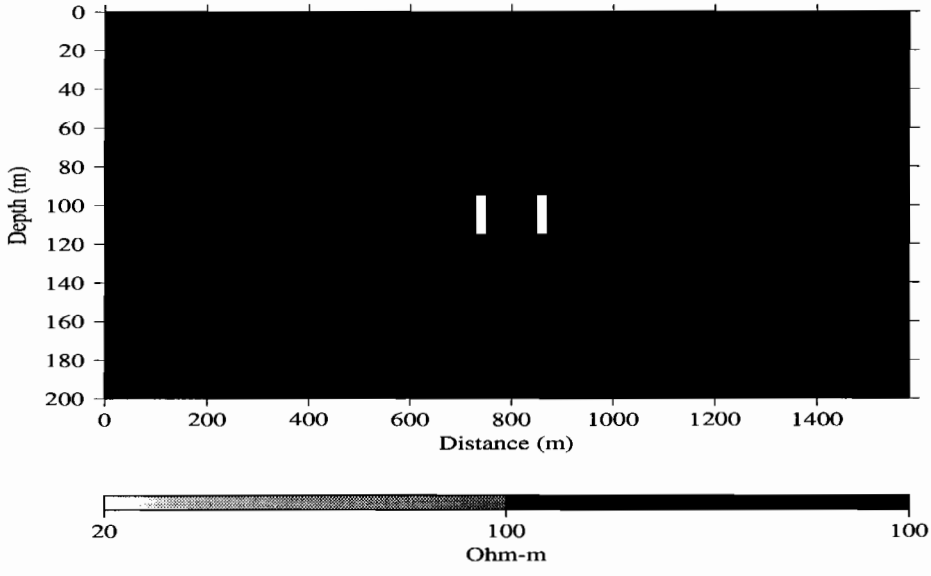

Figure 18: Conductive bodies with 100 m separation.

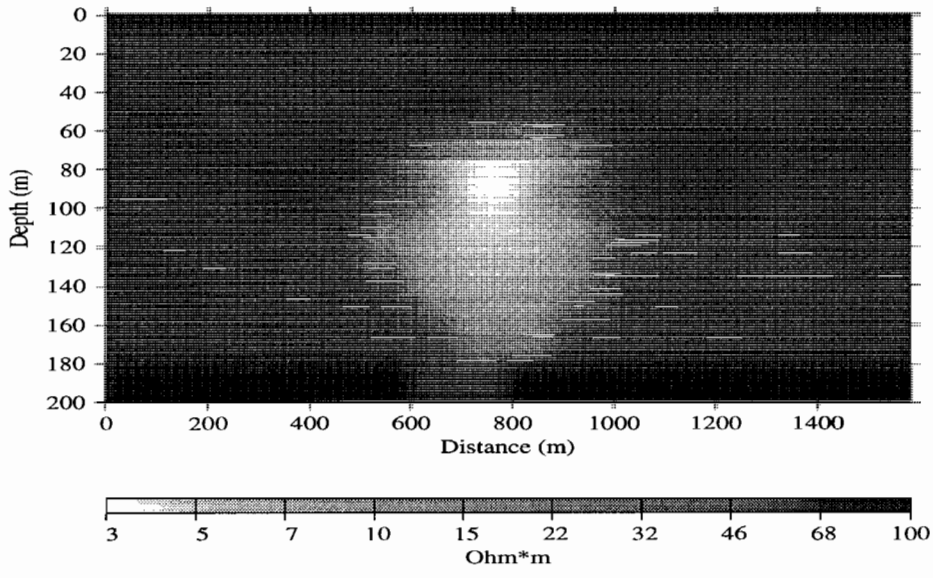

Figure 19: Migration image for conductive bodies with 100 m separation.

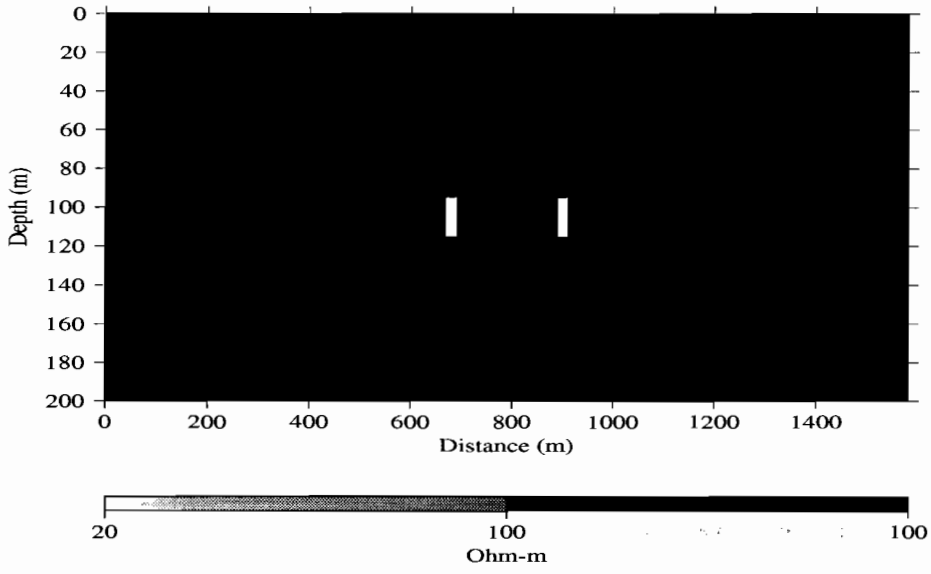

Figure 20: Conductive bodies with 200 m separation.

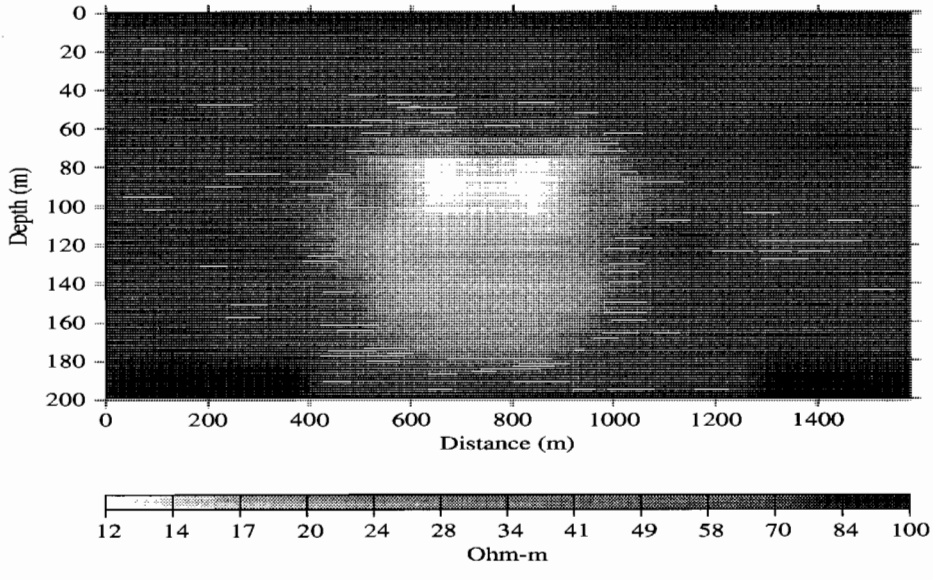

Figure 21: Migration image for conductive bodies with 200 m separation.

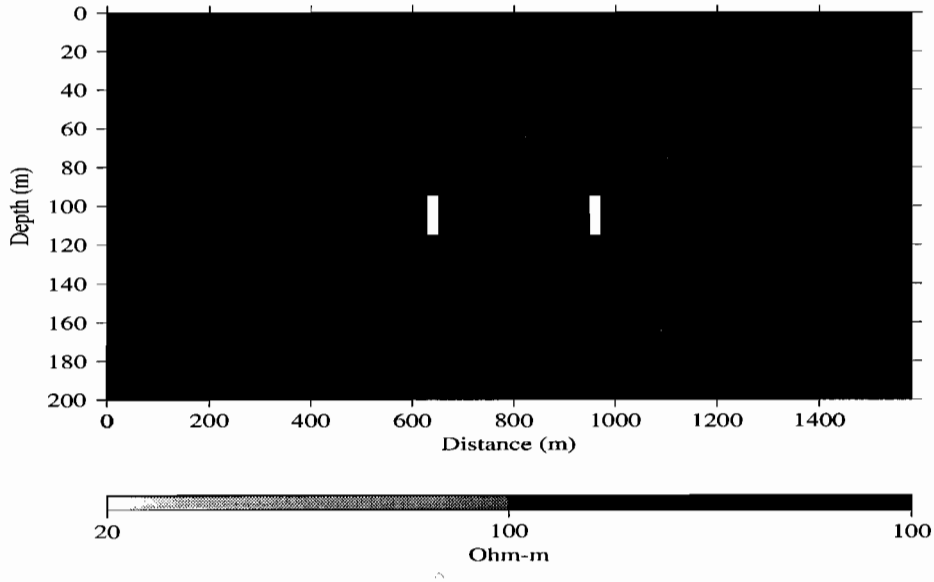

Figure 22: Conductive bodies with 300 m separation.

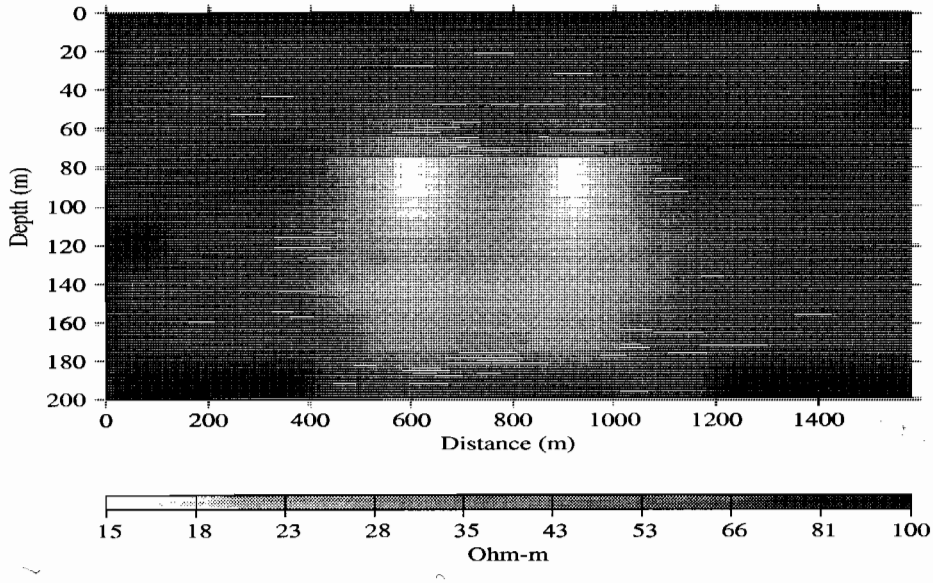

Figure 23: Migration image for conductive bodies with 300 m separation.

homogeneous medium of resistivity 100 Ohm-m at the depth of 100 m. The separation between the two bodies is 300 m (the resolution distance for two bodies as shown by the previous set of models). The geoelectrical cross section of the model is shown in Figure 24. The migration apparent resistivity image in Figure 25 gives a good estimation of the bodies' location, dimensions and resistivity. Of course it is more difficult to see the resistive body on the migration image, because the conductive body is "illuminated" much more brightly. The model presented in Figure 26 is similar to the previous one, but now the resistive body is located at a depth of 50m from the surface, whereas the conductive body is located at 110 m under the surface. The migration apparent resistivity image in Figure 27 gives again a good estimation of the bodies' location, dimensions and resistivity. Thus, migration can be used not only for detecting a highly conductive structure but a resistive structure as well.

3.7 Background resistivity influence on the EM migration image

One of the requirements of the migration method is a knowledge of the background resistivities. Until now, we have used for the migration of our models the true background resistivity. However, in real cases it is not usually known well and can only be approximately estimated. In order to examine the dependence of the migration results on the choice of background resistivity, we have applied the migration with a different background resistivity. The model used in this test is that of one conductive and one resistive body (Figure 24). The migration apparent resistivity image obtained for this model using the "true" resistivity (100 Ohm-m) is shown in Figure 25. The migration images for the same model computed with the background of 80 and 300 Ohm-m are shown in Figure 28 and 29 respectively. In these cases, the position of the two bodies is shifted upwards or downwards. This effect is very similar to the one known in seismic migration. This is why velocity analysis is an important part of seismic data processing before migration. In EM migration, it is also important to correctly determine the background resistivity in order to obtain best results. One approach to this problem is discussed in the paper by Traynin (1995).

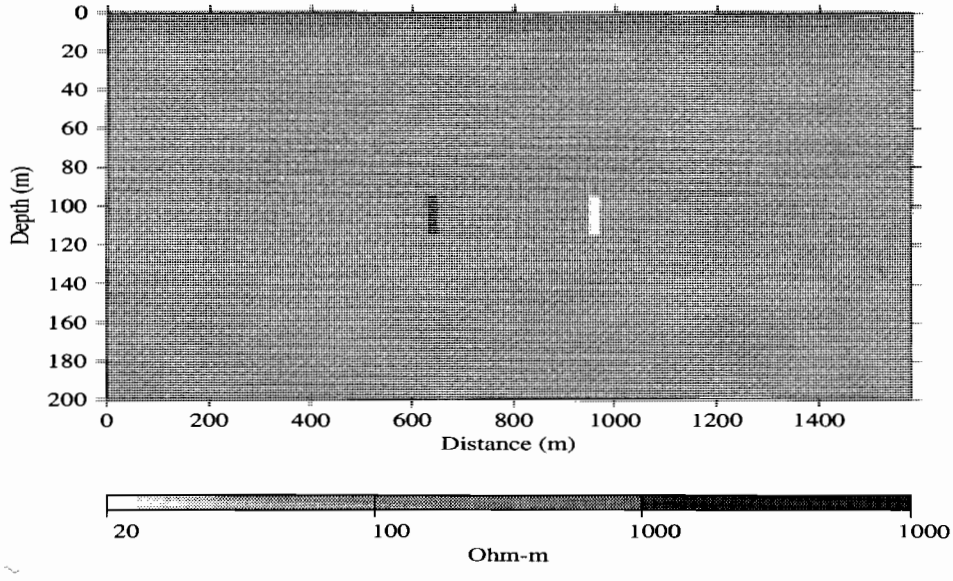

Figure 24: Resistive and conductive bodies with 300 m separation.

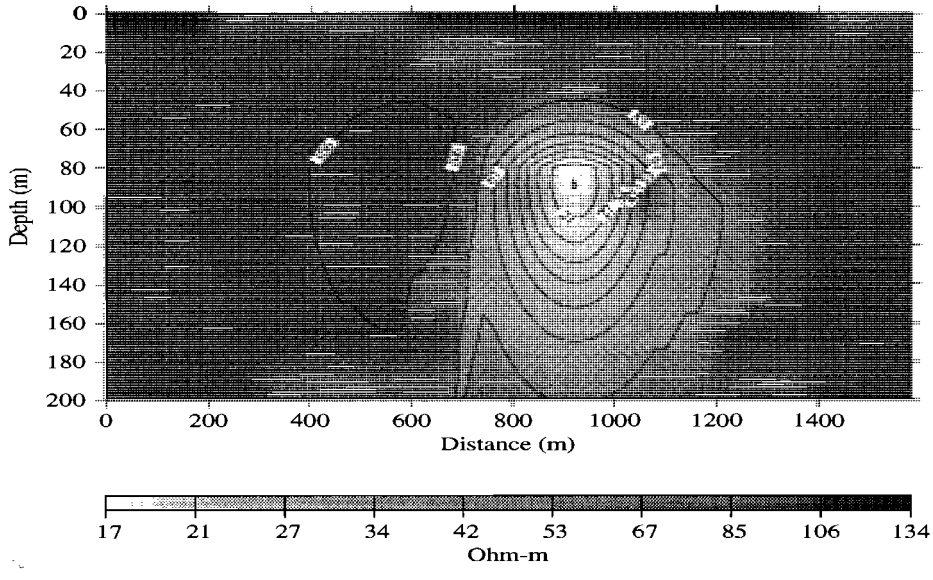

Figure 25: Migration image for resistive and conductive bodies with 300 m separation.

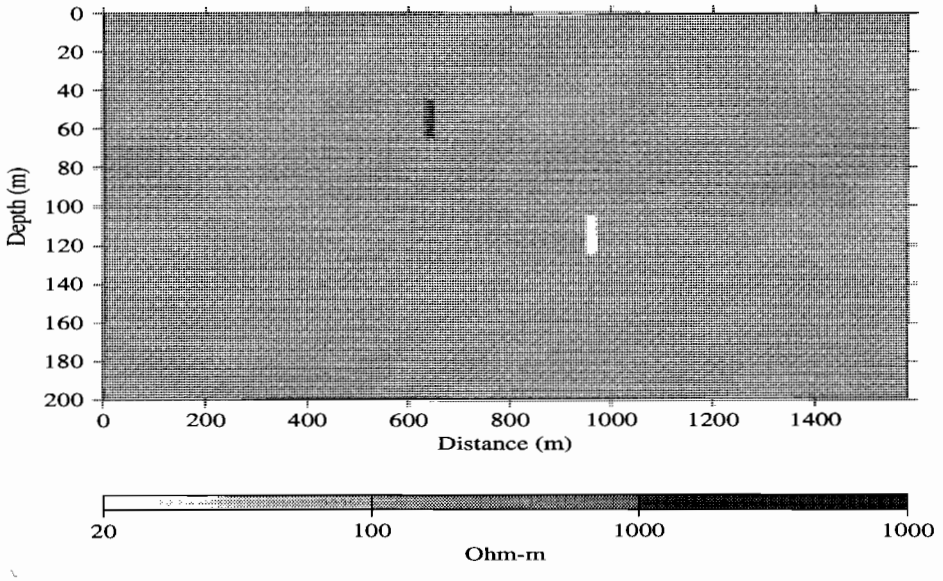

Figure 26: Conductive and resistive body located at different depths.

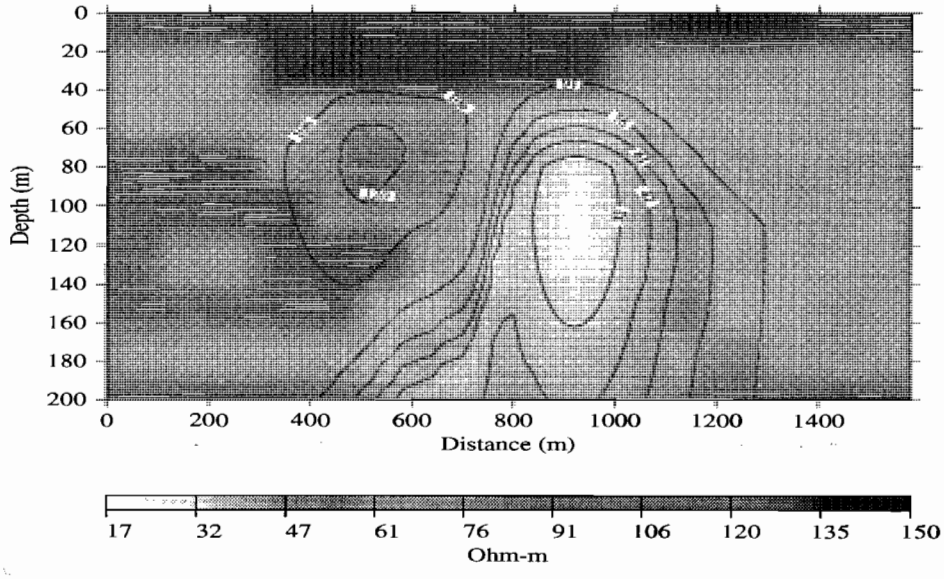

Figure 27: Migration image for model with conductive and resistive bodies located at different depths.

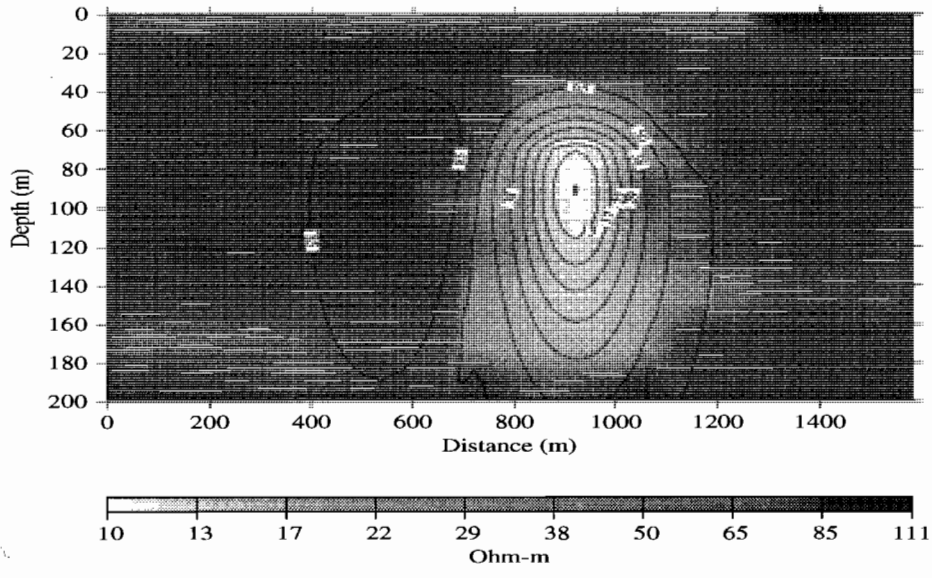

Figure 28: Migration with incorrect background resistivity (80 Ohm-m).

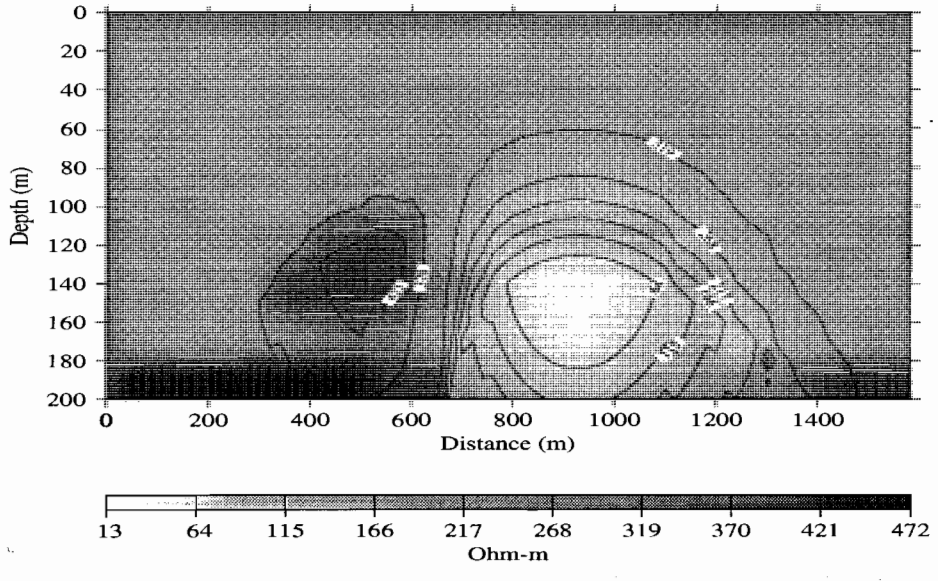

Figure 29: Migration with incorrect background resistivity (300 Ohm-m).

4. EM MIGRATION IN WASTE SITE CHARACTERIZATION

This section describes the application of TDEM migration to the characterization of a US DOE waste site. A large volume of TDEM data was gathered over an existing DOE buried waste facility, the Cold Test Pit, where the location of targets was specified. Transmitting loops that were comparable in size to the targets were used for the TDEM survey. Because of this, 1D interpretation fails to resolve separate objects, but it does provide a reasonable estimation of the background resistivity. The data, however, reflect the lateral location of the targets, thus indicating that more information could be potentially extracted. Since the nature of migration is essentially multidimensional, it was hoped that its application could better resolve the targets. Each profile was migrated separately. After that a composed 3D image of the Pit was constructed. Migration not only resolved separate objects laterally, but also provided reasonable vertical resolution and estimation of anomalous resistivity.

4.1 INEL Waste Complex Characterization Project

Nonintrusive methods of characterizing waste sites and waste forms at U.S. Department of Energy (DOE) operational areas were investigated through a subtask of Technical Task Plan (TTP) AL911201, "Nonintrusive Sensing of Environmentally Significant Objects and Sites" (Chem-Nuclear Geotech 1992a). The subtask (AL911201-G2, "Three-Dimensional Site Characterization Using Broadband Electromagnetics") was developed to investigate various broadband electromagnetic (BBEM) systems that potentially could characterize DOE waste sites in a 3D sense and to demonstrate promising systems under actual field conditions. The BBEM methods investigated were intended not only to locate conductive objects and zones but also to locate accurately the lateral and vertical boundaries of the conductive zones, measure the thickness of any capping material, and provide a qualitative estimate of the type of

waste contained in a particular pit.

A full-scale field demonstration of the PROTEM 47 system at an existing DOE waste site facility was proposed. The Buried Waste Integrated Demonstration (BWID) supported this demonstration at three waste sites in the Radioactive Waste Management Complex (RWMC) at the Idaho National Engineering Laboratory (INEL).

4.2 Survey design and data description

The locations of objects in the Pit were known a priori, which provided an opportunity to check interpretation results. The Pit contains conductive objects simulating waste. The location of the objects is shown in Figure 30. Overall, the Pit possesses two important features, namely conductive objects located near the 0s (South) profile and a conductive zone near the 35s profile. Objects (stacked conductive drums) were buried at depths from 3-5 m.

BBEM survey traverses were conducted over a grid consisting of 5 m spaced traverse lines crossing the Pit. The grid was extended over a sufficiently large area to cover the region of interest. The survey was conducted in the transmitter offset or slingram mode as described in MacLean (1993) and as illustrated in Figure 31. In this mode of operation, the transmitter and receiver coils are offset by a fixed distance. The receiver is placed outside of the transmitter loop and is separated from the nearest side of the loop by a distance of 10 m. The reading point is taken at the midpoint of the two coils, because of the reciprocal relation between transmitter and receiver.

Unlike FDEM systems, the coil separation is not critical to the depth of investigation because the primary or inducing current is off during the measuring period. For the same reason, the TDEM system is not sensitive to noise and signal variations caused by small changes in the system geometry.

TDEM readings were taken over a broad range of time delays on these lines at 2 m intervals. The initial set of readings was recorded over the earliest available series of 20 time delay windows. This initial data set was reviewed in the field; additional data sets at longer time delays were recorded if a measurable signal was observed.

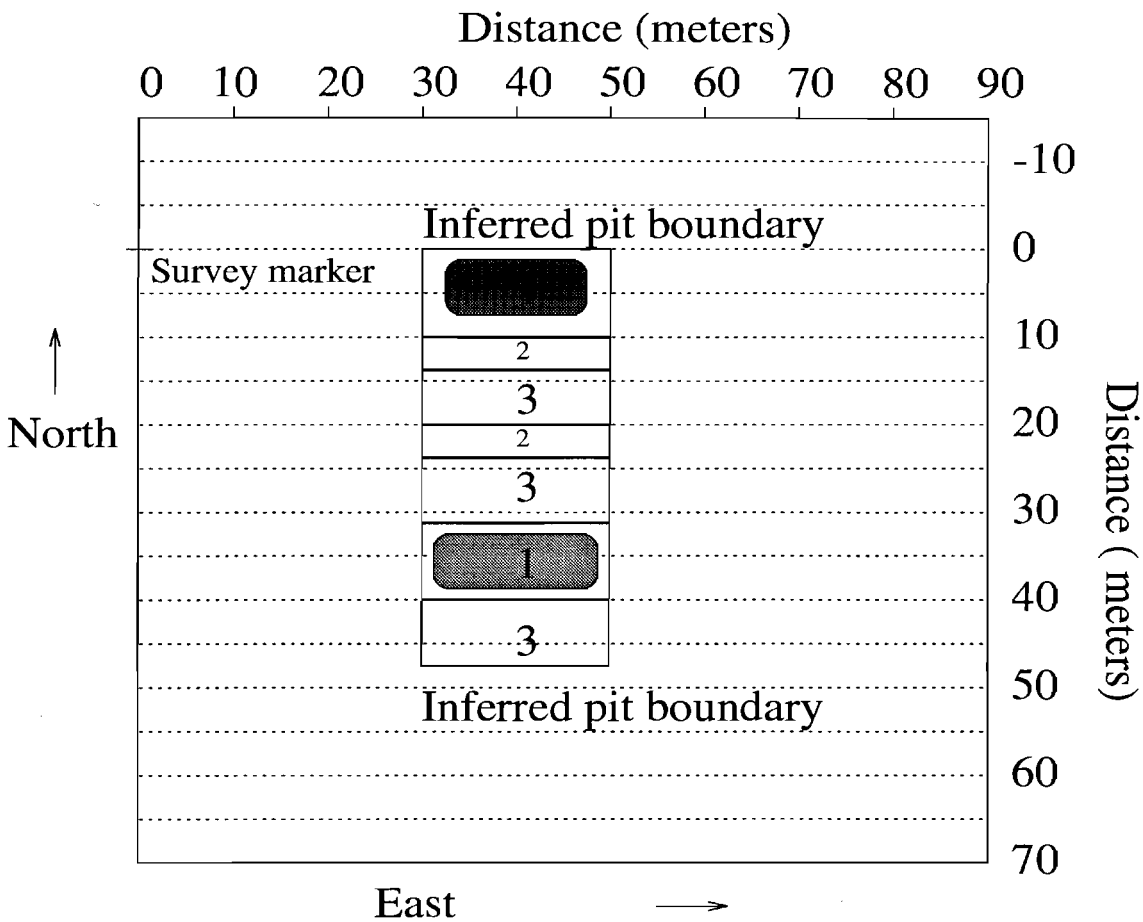

Figure 30: Location of anomalous objects in Cold Test Pit.

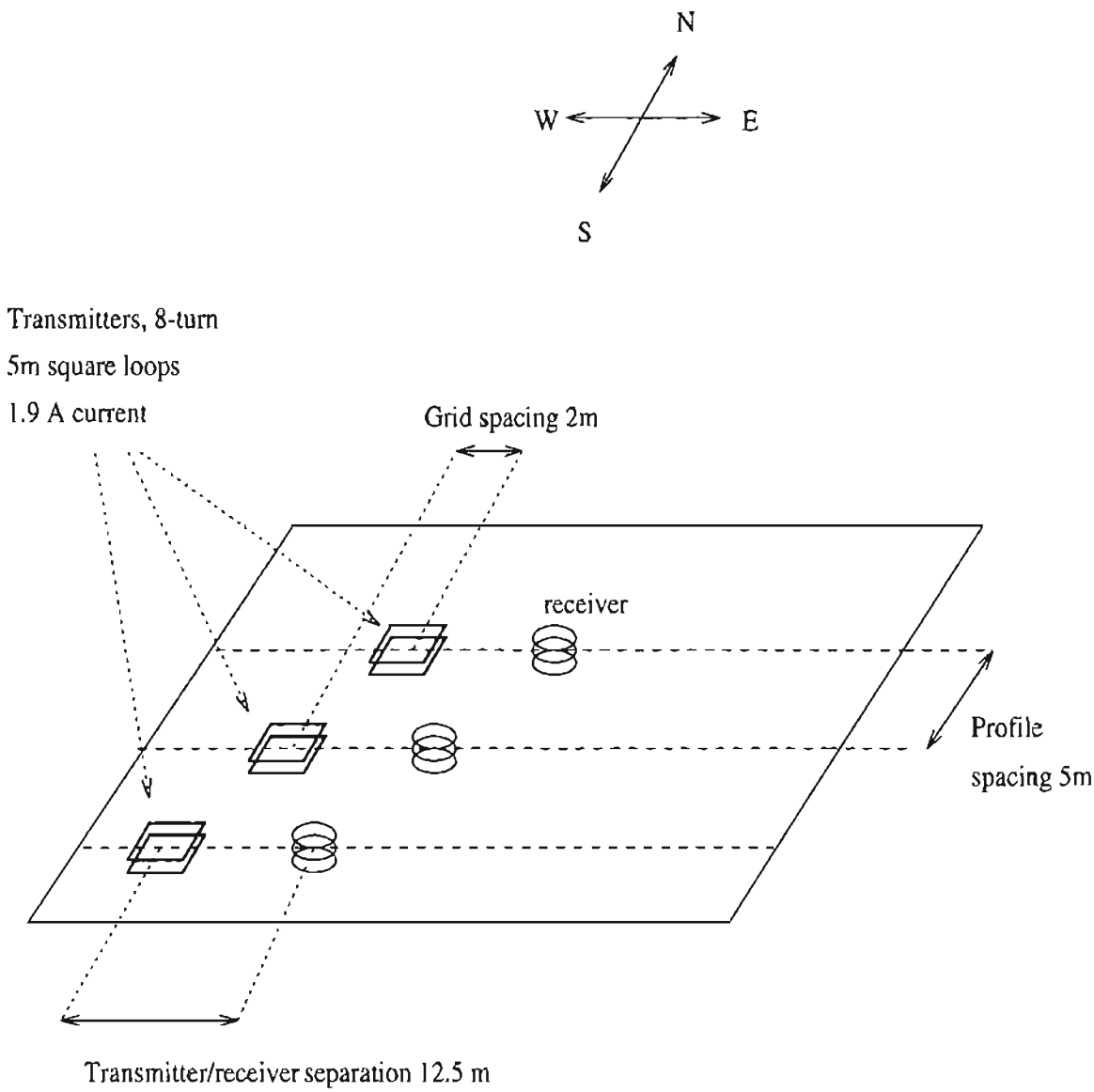

Figure 31: Slingram mode TDEM survey design at Cold Test Pit.

The BWID Cold Waste Pit was covered by the profiles located 5 m from each other. The grid for the Cold Test Pit survey is shown in Figure 30. Two samples of collected data are represented in Figure 32 and Figure 33. We can see from these figures the clear anomaly within the pit borders. Figure 32 presents the total field while Figure 33 presents the secondary field, which was separated using the algorithm described in subsection 3.3.

The "smoke ring" image, obtained using the program written by Eaton and Hohmann, (1989) is presented in Figure 34. The conductive zone is outlined laterally in Figure 34, but no vertical resolution is achieved. The image starts below 4 m depth, because according to the 1D assumption which is the basis of "smoke ring" concept, there is no information in the data above 4 m. The upper part of the image is distorted for the same reason. On the part of the profile without the anomaly, at a depth of 6 m the resistivity is about 100 Ohm-m. This value was taken as the background resistivity for the migration procedure.

1D inversion for these data was also done by MacLean, (1993). No vertical resolution was achieved.

Having a known background resistivity, in spite of random noise, these data have sufficient quality to be migrated.

4.3 Application of migration for data interpretation

Thirteen profiles were processed, numbered from the North to the South (see Figure 30): 15n, 0s, 5s, 10s, 15s, 20s, 25s, 30s, 35s, 40s, 45s, 50s, 60s. An effective background resistivity of $\rho_n = 100\ Ohm - m$ was used. As a result of processing the TDEM data by the migration method a set of vertical cross sections in the Cold Test Pit was obtained. Cross sections of migration apparent resistivity along the profiles 0s and 35s (see Figure 30) are presented in Figure 35 and Figure 36. We can clearly see not only the lateral extent of the anomalous targets, but also the vertical extent of the bodies, which is better than the results obtained by 1D interpretation. The profile images have been interpolated horizontally to obtain the 3D resistivity volume image of the Pit. As an example, the maps of resistivity at the depth 3 and 5 m are

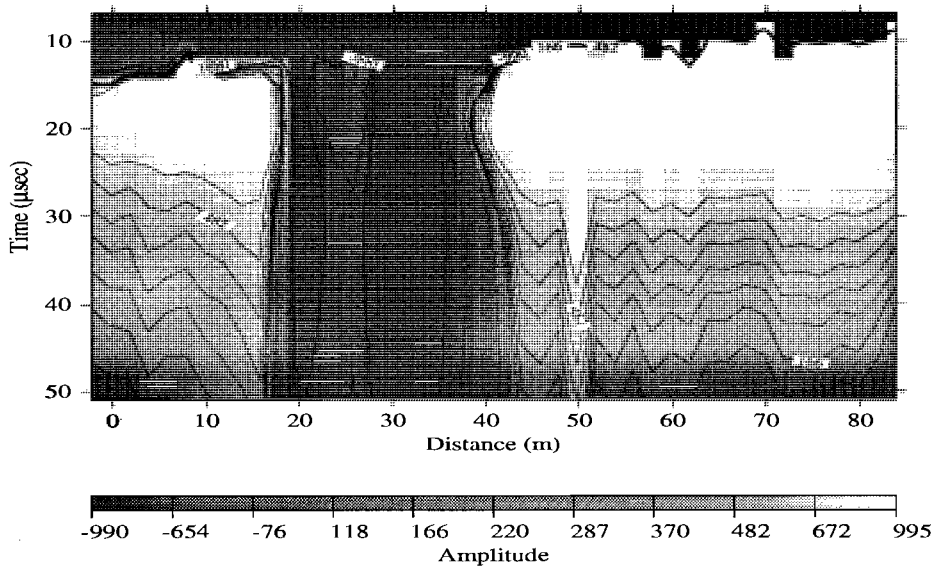

Figure 32: Cold Test Pit TDEM data (profile 0s).

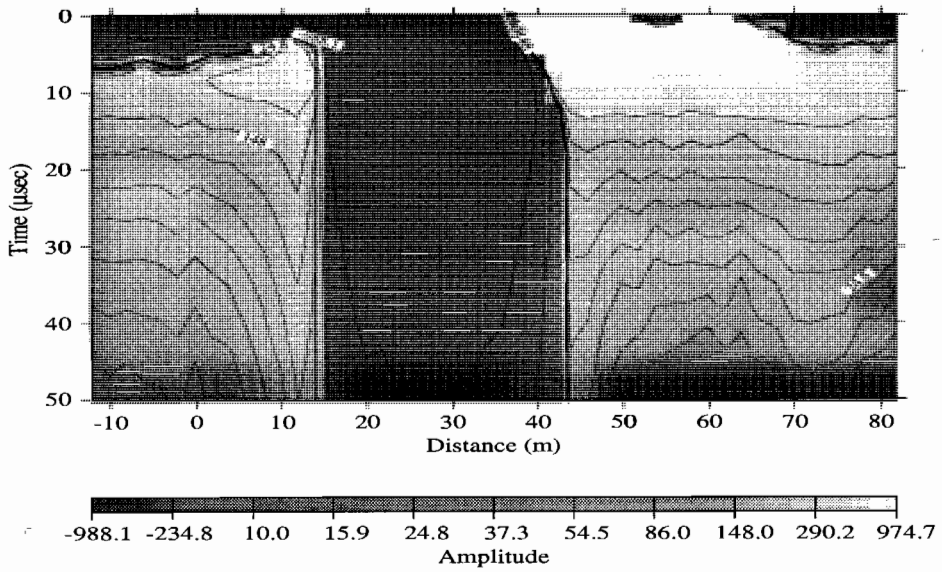

Figure 33: Cold Test Pit TDEM data (profile 35s).

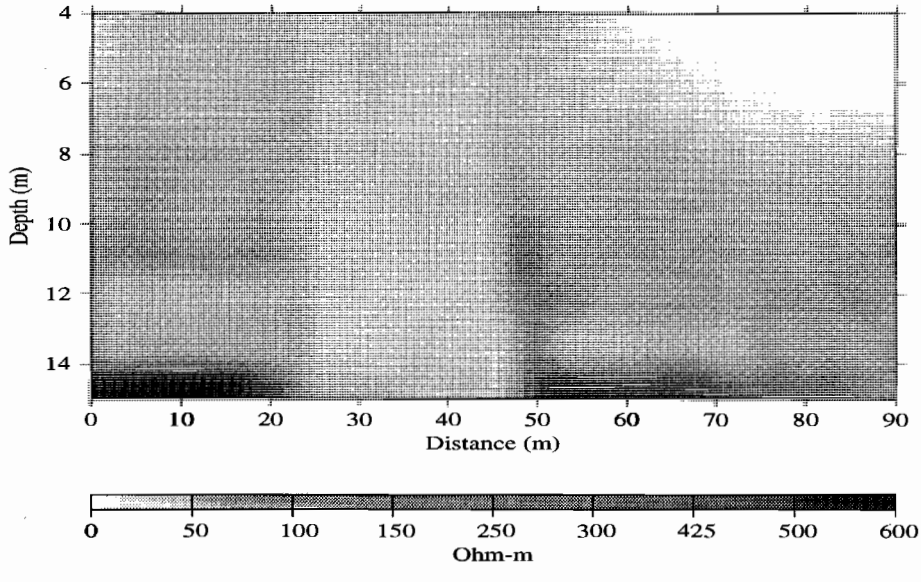

Figure 34: "Smoke ring" image of 0s profile.

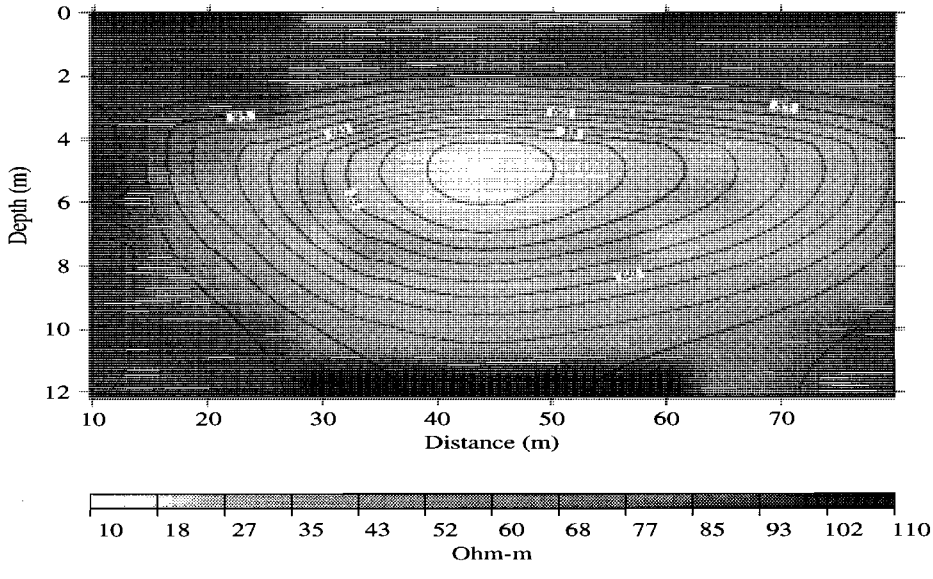

Figure 35: Migration apparent resistivity for Cold Test Pit (profile 0s).

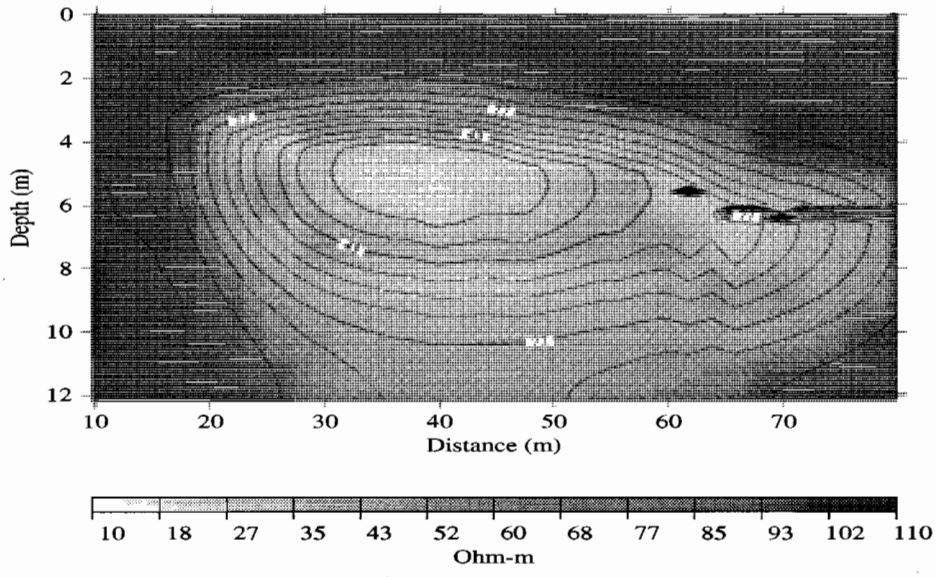

Figure 36: Migration apparent resistivity for Cold Test Pit (profile 35s).

presented in Figure 37 and Figure 38.

The heavy lines on these maps show the known boundary of the pit. Let us analyze, for example, the migration resistivity map at the 5 m depth (Figure 38). We observe on this map several conductivity anomalies that correlate very well with the pit's sections filled with the drums and boxes. Note that elongation of the conductive anomalous zone in the northern section of the pit outside the formal boundary of the pit (shown as a solid line) could be explained as an interpolation effect, since there is no profile in between profiles 15n and 0s.

A 3D image was obtained from the set of 2D profiles using simple linear interpolation. Thus, the conductive structure from profile 0s could be formally extrapolated outside the pit by the interpolation code. However, comparing the map on Figure 38 with the known overall Pit scheme (Figure 30) we can see that in general the principal boundaries of the pit and its internal structure, that is the two characteristic conductive zones along the profiles 0s and 35s and the slightly conductive zone along 15s are reasonably well represented on this map.

Also, 3D resistivity images were constructed on the basis of resistivity maps at the depth 3, 5, 7 and 9 m (see Figure 39). One can see on this map that conductive structures appear near 3 m deep, and disappear between 7 and 9 m deep. The maximum of the conductive structures on the resistivity images lies at the depth about 5 m. These pictures provide a reasonable volume image of the bulk Pit conductivity.

At this point it will be appropriate to outline all the assumptions made in this application. The principal assumption is that TDEM migration theory was developed for the 2D case, yet it was applied to 3D data. We assumed a known background resistivity, while there were no reliable data available for shallow depth range (0-4 m), because the useful image produced by "smoke rings" starts from the 4 m depth. However, comparison of the results of the time domain electromagnetic migration and resistivity imaging with the known object locations demonstrate that this method could be used to determine the structure of anomalous resistivity distributions in the cases where the conductivity distribution is 3D.

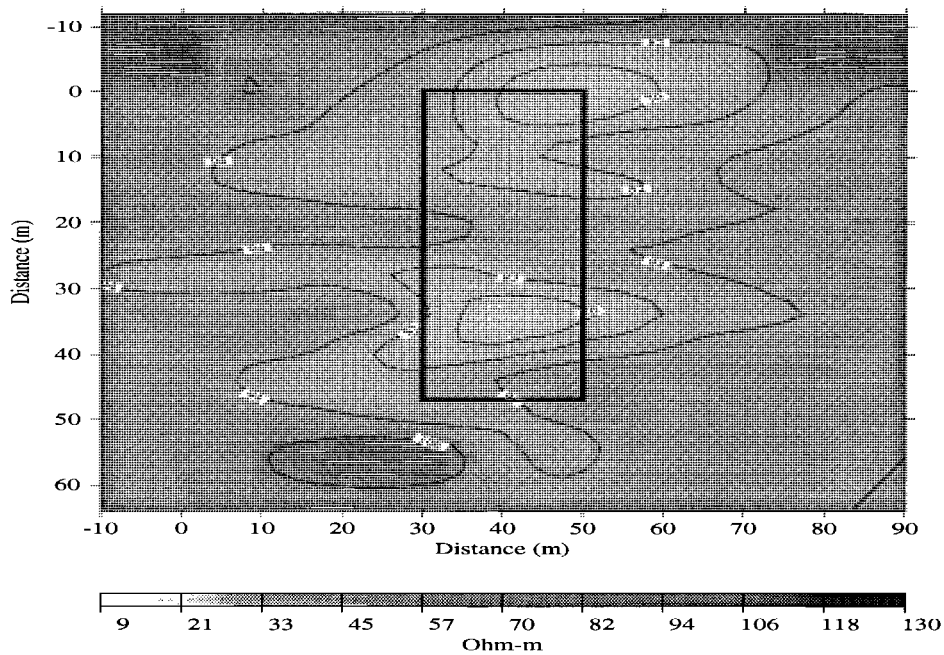

Figure 37: Apparent resistivity map of Cold Test Pit at the depth 3 m.

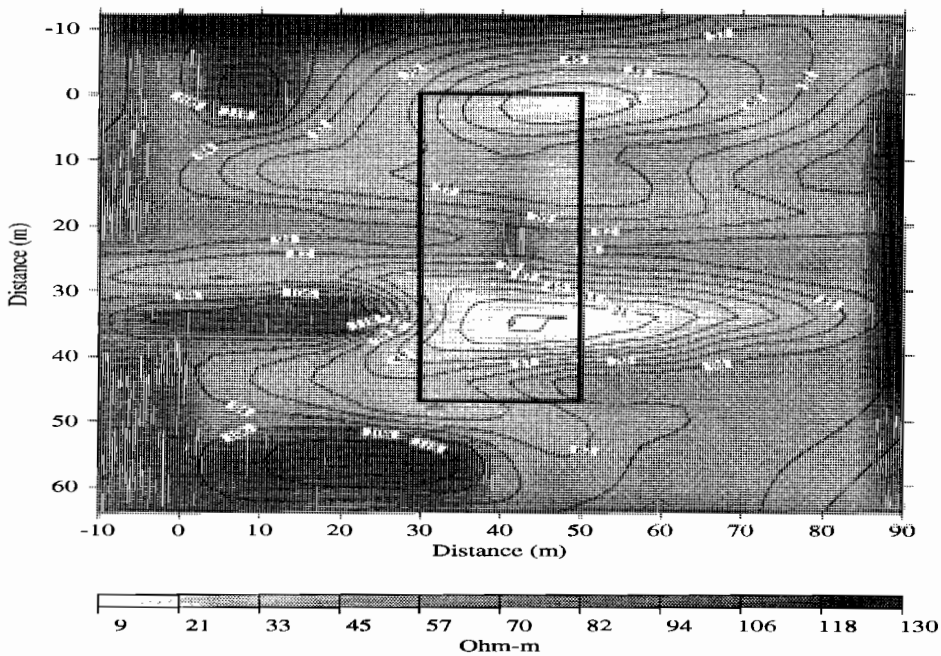

Figure 38: Apparent resistivity map of Cold Test Pit at the depth 5 m.

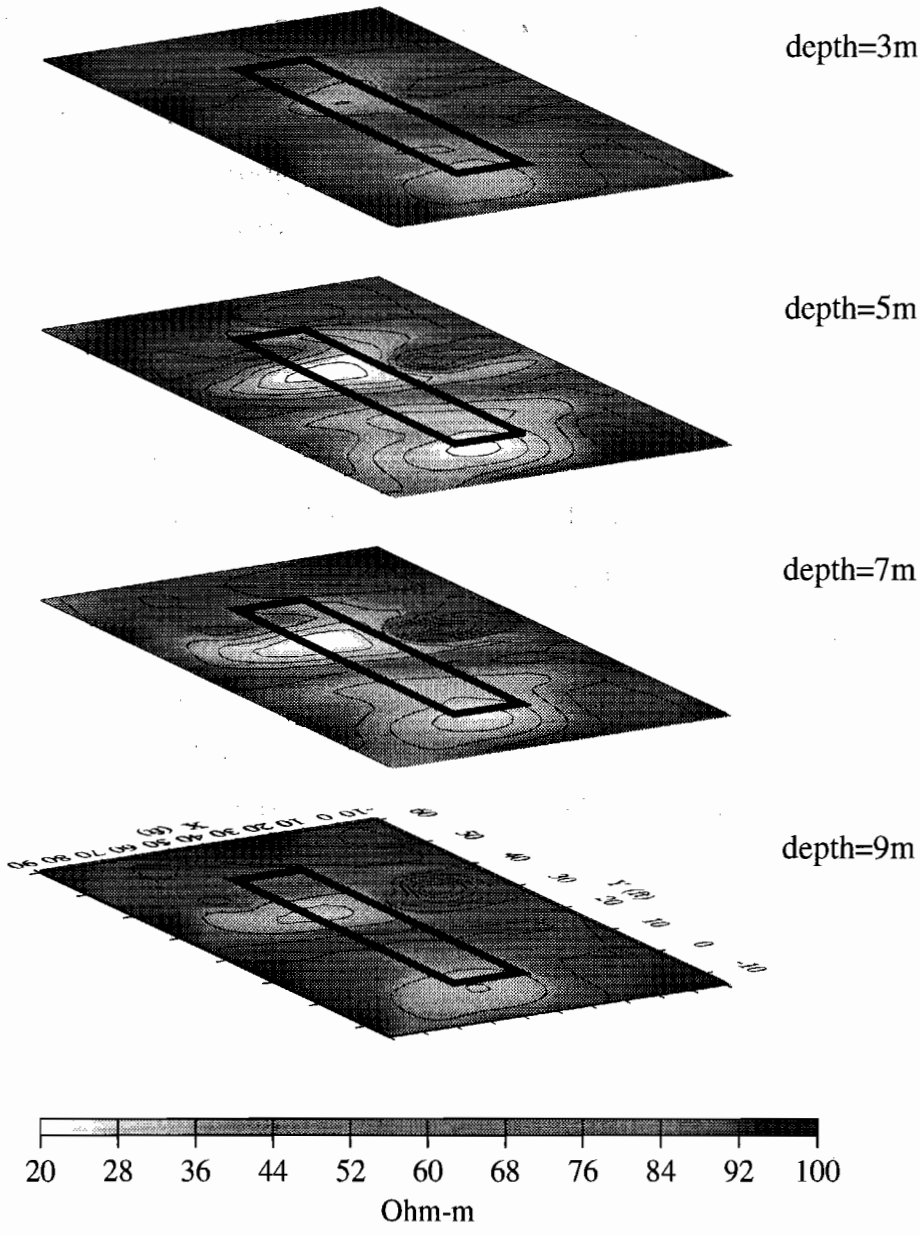

Figure 39: Horizontal slices of Cold Pit resistivity image.

5. CONCLUSION

The main goal of this thesis research was to apply the method of TDEM migration to synthetic and field data. Results suggest that TDEM migration and resistivity imaging make it possible to locate anomalous geoelectric zones and estimate their resistivities. The resistivity images can be obtained from the vertical component of magnetic field H_z, which is the component routinely measured in practice.

The TDEM migration is a stable and fast method of geoelectrical imaging. It provides better resolution of local objects than conventional 1D imaging. It does not require repetitive costly forward modeling as do 2D inversion techniques. The application of migration is limited by the necessity for spatially dense measurements of EM responses along the profile or over an area on the surface of the earth. Errors of estimating the background resistivity affects the accuracy of the migration method.

The results of testing TDEM migration at the Cold Test Pit within the Radioactive Waste Management Complex at the Idaho National Engineering Laboratory demonstrated the method's effectiveness for interpretation of data acquired under real field conditions.

APPENDIX A
APPARENT REFLECTIVITY FUNCTION

The ratio of the primary and secondary fields is equal to the reflection coefficient at a geoelectrical boundary. In the migration concept the actual secondary field is replaced by the field in the reverse time. However, it is still possible to find a reflectivity coefficient using a ratio of migrated secondary field and primary field, as we show here.

Let us consider, for the sake of simplicity the two-layered model with a slowly varying conductivity $\sigma_n(x,z)$ within each layer and a sharp conductivity contrast on the horizontal boundary S between two layers. Consider a 2D model of the electromagnetic field (E-polarization). In a model with a slow horizontal variation of both the conductivity and the field we can represent the different components of the electromagnetic field in the frequency domain approximately by the following formulas (Smith and Booker, 1991; Zhdanov et al., 1994)

$$\begin{aligned} H_z(x,z,\omega) &= Q_z^d(x,z,\omega)e^{ik_n z} + Q_z^u(x,z,\omega)e^{-ik_n z}, \\ H_x(x,z,\omega) &= Q_x^d(x,z,\omega)e^{ik_n z} + Q_x^u(x,z,\omega)e^{-ik_n z}, \\ E_y(x,z,\omega) &= Q_y^d(x,z,\omega)e^{ik_n z} + Q_y^u(x,z,\omega)e^{-ik_n z}, \end{aligned} \tag{33}$$

where the coefficients $Q_{x,y,z}^{u,d}$ vary relatively slowly with the depth, $k_n(x,z,\omega) = \sqrt{i\omega\mu_0\sigma_n(x,z)}$ is a wave number and $\sigma_n(x,z)$ is a background conductivity.

Here the terms associated with the downgoing exponential function correspond to the primary field and the terms associated with the upgoing exponential function correspond to the secondary field:

$$\begin{aligned} H_z^d(x,z,\omega) &= Q_z^d(x,z,\omega)e^{ik_n z}, \quad H_z^u(x,z,\omega) = Q_z^u(x,z,\omega)e^{-ik_n z}, \\ H_x^d(x,z,\omega) &= Q_x^d(x,z,\omega)e^{ik_n z}, \quad H_x^u(x,z,\omega) = Q_x^u(x,z,\omega)e^{-ik_n z}, \\ E_y^d(x,z,\omega) &= Q_y^d(x,z,\omega)e^{ik_n z}, \quad E_y^u(x,z,\omega) = Q_y^u(x,z,\omega)e^{-ik_n z}, \end{aligned} \tag{34}$$

We will analyze the behavior of the horizontal component of the electric field at the quasi-horizontal boundary $\{S:\ (x, d(x))\}$ between two layers. On the first-layer side of the boundary we have:

$$\begin{aligned} E_y(x,d,\omega) &= Q_y^d(x,d,\omega)e^{ik_n d} + Q_y^u(x,d,\omega)e^{-ik_n d}, \\ E_y'(x,d,\omega) &= ik_n Q_y^d(x,d,\omega)e^{ik_n d} - ik_n Q_y^u(x,d,\omega)e^{-ik_n d}, \end{aligned} \tag{35}$$

while on the second-layer side we have:

$$\begin{aligned} E_y(x,d,\omega) &= Q_y(x,d,\omega)e^{ik_{n+1} d}, \\ E_y'(x,d,\omega) &= ik_{n+1} Q_z(x,d,\omega)e^{ik_{n+1} d}, \end{aligned} \tag{36}$$

where "prime" denotes the vertical derivative of the electric field.

On the boundary S in the case of E-polarization both components E_y and E_y' are continuous. Therefore, the corresponding right-hand sides of (35) and (36) are equal. Solving this system of equations, we find:

$$\frac{Q_y^u}{Q_y^d} = \beta(x,d)\, e^{2ik_n d}, \tag{37}$$

where

$$\beta(x,d) = \frac{\sqrt{\sigma_n(x,d)} - \sqrt{\sigma_{n+1}(x,d)}}{\sqrt{\sigma_n(x,d)} + \sqrt{\sigma_{n+1}(x,d)}}, \tag{38}$$

is the *reflectivity coefficient*. The frequency domain apparent reflectivity function as the ratio of the secondary and primary fields is:

$$\beta_{\omega a}(x,z,\omega) = \frac{E_y^u(x,z,\omega)}{E_y^d(x,z,\omega)} = \frac{Q_y^u(x,z,\omega)}{Q_y^d(x,z,\omega)} e^{-2ik_n z}. \tag{39}$$

According to (37) at the boundary:

$$\beta_{\omega a}(x,d,\omega) = \beta(x,d)\,. \tag{40}$$

So. at the geoelectrical boundary the apparent reflectivity function is equal to the true reflectivity coefficient.

Now let us find the way to calculate the apparent reflectivity function from the migrated fields. According to the definition (Zhdanov et al., 1994a), the migrated secondary field is equal to:

$$E_y^{ms}(x,z,\omega) = Q_y^u(x,z,\omega)e^{-k_m z}, \tag{41}$$

and the migrated primary field is equal to:

$$E_y^{mp}(x,z,\omega) = Q_y^d(x,z,\omega)e^{-k_m z}, \tag{42}$$

where $k_m(x,z,\omega) = \sqrt{i\omega\mu_0\sigma_m(x,z)}$ is a migration wave number.

We can introduce the frequency domain migration apparent reflectivity function as :

$$\beta_{\omega a}^m(x,z,\omega) = \frac{E_y^{ms}(x,z,\omega)}{E_y^{mp}(x,z,\omega)} = \frac{Q_y^u(x,z,\omega)}{Q_y^d(x,z,\omega)}. \tag{43}$$

Calculating the ratio of the apparent reflectivity function and migration apparent reflectivity function using (39) and (43) gives:

$$\frac{\beta_{\omega a}(x,z,\omega)}{\beta_{\omega a}^m(x,z,\omega)} = e^{-2ik_n z}. \tag{44}$$

Thus we obtain:

$$\beta_{\omega a}^m(x,z,\omega) = \beta_{\omega a}(x,z,\omega)e^{2ik_n z}. \tag{45}$$

According to eq. (40) at the boundary S :

$$\beta_{\omega a}^m(x,d,\omega) = \beta_{\omega a}(x,d,\omega)e^{2ik_n d} = \beta(x,d)\,e^{2ik_n d}. \tag{46}$$

This means that the migrated secondary and primary fields are proportional at the boundary:

$$E_y^{ms}(x,d,\omega) = \beta\,(x,d)\,E_y^{mp}(x,d,\omega)e^{2ik_n d}. \tag{47}$$

Equation (47) can be used for calculating the time domain migration apparent reflectivity function at zero time :

$$\beta_a^m\,(x,z) = \beta_{ta}^m(x,z,t=0) = \frac{E_y^{ms}(x,z,t=0)}{D(x,z)}. \tag{48}$$

Here $\beta_{ta}^m(x,z,t)$ is the time domain migration apparent reflectivity function obtained from $\beta_{\omega a}^m(x,d,\omega)$ by inverse Fourier transform from the frequency domain to the time domain, and

$$D(x,z) = \int_0^{+\infty} E_y^{mp}(x,z,t)\varphi\,(z,t)\,dt, \tag{49}$$

where

$$\varphi\,(z,t) = a\frac{z}{\tau^3}\exp\left[-2\pi^2\left(\frac{z}{\tau}\right)^2\right], \tag{50}$$

and

$$a = \frac{3^{7/2}\pi^{5/2}}{\mu\sigma_1};\ \tau = 2\pi\sqrt{2t/\mu\sigma_1}. \tag{51}$$

The function $\beta_a^m\,(x,z)$ is equal to the actual reflectivity coefficient β exactly at the position of the boundary:

$$\beta_a^m(x,d) = \beta\,(x,d)\,. \tag{52}$$

APPENDIX B
MIGRATION APPARENT RESISTIVITY

As shown in Appendix A, the apparent reflectivity function is equal to the reflectivity coefficient at a geoelectrical boundary. Substituting a plane wave for the primary field and considering a two-layered model, one can have an expression connecting the reflectivity function with the amplitude of the migrated field. Using this relationship one can express the anomalous resistivity via the migrated field amplitude. Although derived for the plane wave and two-layered model, this expression can be used in the general case, thus leading to a migration apparent resistivity.

Let us consider the model that is based on the assumption that the coefficient $Q_y^d(x,z,\omega)$ in equation (36) does not depend on ω and very slowly changes with z :

$$Q_y^d(x,z,\omega) \approx Q_0(x). \tag{53}$$

These conditions for example take place in the case of constant conductivity of the first layer and if the primary field can be approximated by the plane wave with a $\delta-$pulse waveform on the surface of the earth. Under these conditions we can write approximately:

$$E_y^d(x,z,\omega) = Q_0(x)\, e^{ik_n z}. \tag{54}$$

Therefore from (37) and (36) we have:

$$E_y^u(x,z,\omega) = Q_0(x)\,\beta_{12}(x,d)\, e^{2ik_n d} e^{ik_n z}. \tag{55}$$

According to definition, the migrated secondary field in the frequency domain is equal to

$$E_y^{ms}(x,z,\omega) = Q_0(x)\,\beta(x,d)\, e^{2ik_n d} e^{-k_m z}. \tag{56}$$

If we apply the inverse Fourier transform from the frequency domain to the time-domain, we find the migrated secondary field in the time domain:

$$E_y^{ms}(x,z,t) = \frac{1}{2\pi} Q_0(x)\,\beta(x,d) \int_{-\infty}^{+\infty} e^{2ik_n d} e^{-k_m z} e^{-i\omega t} d\omega. \tag{57}$$

The last integral can be reduced to a tabulated one, if $t = 0$. Omitting long calculations, we write:

$$E_y^{ms}(x,z,t=0) = -\frac{8Q_0(x)\,\beta(x,d)\,d\gamma^{1/2}z}{\pi\mu\sigma_1\left(4d^2+\gamma z^2\right)^2}, \tag{58}$$

where $\gamma = \sigma_m/\sigma_n$ is the migration constant.

Let us find now the depth of the extremum of the migration field. Since

$$\frac{\partial}{\partial z} E_y^{ms}(x,z,t=0) = -\frac{8Q_0(x)\,\beta_{12}(x,d)\,d\gamma^{1/2}z}{\pi\mu\sigma_1\left(4d^2+\gamma z^2\right)^3}\left(4d^2-3\gamma z^2\right), \tag{59}$$

the vertical derivative of the migrated field is equal to zero exactly at the depth of the boundary $z = d$, if the migration constant $\gamma = 4/3$. The value of the migration field in the extremum is equal to

$$E_y^{ms}(x,d,t=0) = -\frac{\sqrt{3}Q_0(x)\beta(x,d)}{4\pi\mu\sigma_m d^2}. \tag{60}$$

From the last formula we can find $\beta(x,d)$

$$\beta(x,d) = -\frac{4\pi\mu\sigma_m d^2}{\sqrt{3}Q_0(x)} E_y^{ms}(x,d,t=0), \tag{61}$$

and calculate the resistivity of the second layer:

$$\rho_{n+1}(x) = \left[\frac{1+\beta(x,d)}{1-\beta(x,d)}\right]^2 \rho_n. \tag{62}$$

Expression (62) gives the exact solution for determining $\rho_{n+1}(x)$ only for the simple model under consideration. However, following a traditional approach to electromagnetic sounding, we can introduce the migration apparent resistivity, which is

determined by the same formula:

$$\rho_m(x,z) = \left[\frac{1+\beta_a^m(x,z)}{1-\beta_a^m(x,z)}\right]^2 \rho_n. \tag{63}$$

In the last expression $\beta_a^m(x,z)$ is given by eq. (48).

Note in the conclusion that expression (61) can be obtained directly from equations (48) and (49).

REFERENCES

Adhidjaja, J.I., Hohmann, G.W. and Oristaglio, M.L., 1985, Two-dimensional transient electromagnetic responses, Geophysics, **50**, 2849-2861.

Barnett, C.T., 1984, Simple inversion of time-domain electromagnetic data, Geophysics, **49**, 925-933.

Berdichevsky, M.N., and Zhdanov, M.S., 1984, Advanced theory of deep geomagnetic sounding, Elsevier, Amsterdam.

Cai, W., Qin, F., and Shuster, G.T., 1995, Electromagnetic velocity inversion using two-dimensional Maxwell's equations, submitted to Geophysics.

Claerbout, J.F., and Doherty, S.M., 1972, Downward continuation of moveout-corrected seismograms, Geophysics, **37**, 741-768.

Claerbout, J.F., 1985, Imaging the earth's interior, Blackwell Sci. Publ., Oxford,Eng.

Eaton, P.A., and Hohmann, G.W., 1989, A rapid inversion technique for transient electromagnetic soundings, PEPI, **53**, 384-404.

Farquharson, C.G., and Oldenburg, D.W., 1993, Inversion of time-domain electromagnetic data for a horizontally layered earth, Geophys. J. Int., **144**, 433-442.

Lee, S., McMechan, G.A., and Aiken, L.V., 1987, Phasefield imaging: The electromagnetic equivalent of seismic migration, Geophysics, **52**, 679-693.

Macnae, J., and Lamontagne, Y., 1987, Imaging quasi-layered conductive structures by simple processing of transient electromagnetic data, Geophysics, **52**, 545-554.

MacLean, H.D., 1993, Time domain electromagnetic survey of three waste burial pits at INEL radioactive waste management complex, TTP AL 911201-G2, Chem-Nuclear Geotech, Inc.

Morse, P.M., and Feshbach, U., 1953, Methods of theoretical physics, McGrawHill Book Co., New York.

Nabighian, M.N., 1979, Quasi-static transient response of a conducting half-space - an approximate representation, Geophysics, **44**, 1700-1705.

Oristaglio, M., and Hohmann, G., 1984, Diffusion of electromagnetic fields into a two-dimensional earth: A finite-difference approach, Geophysics, **49**, 870-894.

Schneider, W.A., 1978, Integral formulation for migration in two and three dimensions, Geophysics, **43**, 49-76.

Smith, J.T., and Booker, J.R., 1991, Rapid inversion of two- and three-dimensional inversion of magnetotelluric data, J. Geoph. Res.,**96**, 3905-3922.

Tarantola, A., 1987, Inverse problem theory. Methods for data fitting and model parameter estimation, Elsevier,Amsterdam.

Traynin, P.N., 1995, Analysis of rapid inversion techniques and time-domain electro-

magnetic migration results for transient electromagnetic soundings, In preparation.

Xiong, Z., 1992, Electromagnetic modelling of three-dimensional structures by the method of system iterations using integral equations, Geophysics, **57**, 1556-1561.

Zhdanov, M.S., and Frenkel, M.A. 1983, Migration of electromagnetic fields in the solution of geoelectrical inverse problems, Doklady Akademii Nauk SSSR, N3, **271**, 589-594.

Zhdanov, M.S., and Frenkel, M.A., 1983a, Electromagnetic migration. The development of the deep geoelectric model of the Baltic Shield, Oulu (Finl.): University of Oulu, part 2, 37-58.

Zhdanov, M.S., and Frenkel, M.A., 1983b, The solution of the inverse problems on the basis of the analytical continuation of the transient electromagnetic field in reverse time, J.Geomagn. and Geoelec., **35** 747-765.

Zhdanov, M.S., 1988, Integral transforms in geophysics, Springer-Verlag, New York.

Zhdanov, M.S., Matusevich, V.U., and Frenkel, M.A., 1988, Seismic and electromagnetic migration, (in Russian) Nauka, Moscow.

Zhdanov, M.S. and Podchufarov, V.V., 1988, Migration of scalar components of electromagnetic fields for geoelectrical problems, Dokladu Akademii Nauk SSSR, N3, **299**, 331-335.

Zhdanov, M.S., and Booker, J.R., 1993, Underground imaging by electromagnetic migration, SEG Expanded Abstracts 63rd Annual meeting, Washington D.C., 355-357.

Zhdanov, M.S., and Keller, G.V., 1994, The geoelectrical methods in geophysical exploration, Elsevier, Amsterdam.

Zhdanov, M.S., Traynin, P., and Booker, J.R. , 1994a, Principles of electromagnetic migration, (submitted to Geophysics).

Zhdanov, M.S., Traynin, P., and Portniaguine, O., 1994b, Migration and analytic continuation in geoelectric imaging, SEG 64th Annual Meeting, Expanded Abstracts, Los Angeles, 357-360

Zhdanov, M.S., Traynin, P., and Portniaguine, O., 1995a, Resistivity imaging by time domain electromagnetic migration (TDEMM), (submitted to Exploration Geophysics).

Zhdanov, M.S., Traynin, P., Portniaguine, O.N., and MacLean, D. 1995b, Time domain electromagnetic migration in INEL RWMC Cold Test Pit characterization, Proceedings of the Symposium on the Applications of Geophysics to Engineering and Environmental Problems, SAGEEP 95, Orlando, Fl., 919-924.